

ASSESSMENT OF POLARIMETRIC METHODOLOGIES FOR BACKSCATTERED
IMAGING IN TURBID MEDIA

A Thesis

Presented to

The Graduate Faculty of The University of Akron

In Partial Fulfillment

of the Requirements for the Degree

Master of Science

Kamalakar Ambadipudi

May, 2009

ASSESSMENT OF POLARIMETRIC METHODOLOGIES FOR BACKSCATTERED
IMAGING IN TURBID MEDIA

Kamalakar Ambadipudi

Thesis

Approved:

Accepted:

Advisor
Dr. George C. Giakos

Department Chair
Dr. Daniel B. Sheffer

Committee Member
Dr. Daniel B. Sheffer

Dean of the College
Dr. George K. Haritos

Committee Member
Dr. Dale H. Mugler

Dean of the Graduate School
Dr. George R. Newkome

Date

ABSTRACT

In optical imaging, the high random scattering of light in biological tissue can degrade the contrast of an image which could be a drawback in detection of tumors. Polarization based imaging has shown its capability in overcoming such drawbacks over the recent years. It depends on discrimination of randomly polarized light from weakly polarized light yielding an enhanced image contrast. The purpose of this research study was to investigate, compare and assess the imaging potential of two widely used techniques in the field of polarimetric imaging namely, Linear Polarimeter method (uses linearly polarized light) and Rotating Retarder Polarimeter method (uses circularly polarized light) to interrogate targets embedded in turbid biological media. This novel study may contribute to early detection of diseases and pathologies in biological tissues.

The polarization properties of the backscattered light from a turbid medium containing a target submerged in a scattering solution were studied. A preclinical optical phantom was designed and the experiments were done in two phases, each phase corresponding to a different polarimetric technique. Specifically, a polystyrene cylinder was used as the target and the turbid medium was simulated by adding skim milk in volume percentage increments in both the phases. The first phase of experiments involved the Rotating Retarder Polarimeter method and the Polarimetric Measurement Matrix Reduction techniques. The images obtained by this method were processed by

means of a data reduction algorithm, based on Polarimetric Measurement matrix method to calculate the Degree of Linear Polarization (DOLP) image and total intensity (S_0) image. The second phase of experiments involved the Linear Polarimeter method. The resulting co-polarized and cross-polarized images from this method were processed to obtain Degree of Polarization (R_{pol}) images. Both of these experiments were performed using a backscattered polarimetric imaging system.

The images obtained by both the techniques were analyzed by computing signal to background ratio (SBR) values and number of pixels detected as edges for every concentration of skim milk solution added to the surrounding medium of the target. The obtained images were then compared to determine the image quality.

Experimental results from both these techniques showed that the DOLP images obtained by the Rotating Retarder Polarimeter method provide better contrast in terms of signal to background ratio (SBR) values and number of pixels detected as edges compared to Degree of Polarization (R_{pol}) images obtained by the linear Polarimeter method. Overall, the contributions of this study suggest that the interrogation of targets in turbid media using circularly polarized light exhibits superior imaging characteristics with respect to linearly polarized light interrogation.

DEDICATION

This work is dedicated to my Parents and Friends

ACKNOWLEDGEMENTS

At this point I must thank Dr. George C. Giakos for the support he has shown me during my Master's. Without his constant advice and guidance this research would have been extremely difficult. I would also like to thank his family for treating us as their own family members.

I must also thank members of my committee, Dr. Daniel Sheffer and Dr. Dale Mugler for their valuable suggestions. They have been extremely patient helping me with the thesis and very kind with their presence.

Having a friend in Keerthi Valluru is a blessing I was bestowed upon. He is the most sincere, hardworking and caring person I have ever met. I would also like to thank Dyuti trivedi and Eisenhut family for being there with me through my hard times. Having friends like Keerthi, Dyuti, Don and Melinda is what I consider a true friendship should be.

Finally I must thank the entire staff at Zee's which is a second family for me here in Akron. I would also like to thank everyone who has helped me directly or indirectly in completion of this research.

TABLE OF CONTENTS

	Page
LIST OF TABLES	x
LIST OF FIGURES	xii
CHAPTER	
I. INTRODUCTION	1
1.1 Overview	1
1.2 Purpose of Study	2
1.3 Objectives of study	3
1.4 Research Hypotheses	3
1.4.1 Null hypotheses	3
1.4.2 Alternate hypotheses	4
1.5 Limitations of the Study	4
II. LITERATURE REVIEW	5
2.1 Optical Imaging	5
2.2 Polarimetry based optical imaging	7
2.3 Polarized Light	8
2.4 Stokes Parameters	10
2.5 Polarimetric imaging parameters	11
III. METHODS AND PROCEDURES	12

3.1 Design of Phantom	12
3.2 Experimental Setup	13
3.3 Experimental Procedures.....	15
3.3.1 The Rotating Retarder Polarimeter Experimental Setup	15
3.3.2 The Linear Polarimeter Experimental Setup	16
3.4 Alignment and Calibration Procedures	17
3.5 Image Processing.....	18
3.6 Analysis Techniques	19
IV. MATERIALS USED.....	21
4.1 Optical Table Top.....	21
4.2 Laser Source	21
4.3 Neutral Density Filter.....	22
4.4 Linear Polarizers	22
4.5 Quarter wave Retarders.....	22
4.5.1 Berek Polarization Compensator	23
4.5.2 Quartz Quarter Wave Retarder	23
4.6 Beam expander	24
4.7 CCD Camera	25
V. RESULTS AND DISCUSSIONS.....	26
5.1 Results of the Rotating Retarder Polarimeter method.....	26
5.2 Results of the Linear Polarimeter Method	38
5.3 Discussion	45
VI. CONCLUSIONS AND FUTURE WORK.....	53

REFERENCES	54
APPENDIX.....	58

LIST OF TABLES

Table	Page
4.1 Specifications of Laser Source.....	21
4.2 Specifications of the Polarizers.....	22
4.3 Specifications of the Berek compensator.....	23
4.4 Specifications of the Quarter wave Retarder	24
4.5 Specifications of the Beam Expander	24
4.6 Specifications of the CCD camera.....	25
5.1 SBR values of DOLP images obtained for Skim Milk solution in the Rotating Retarder Polarimeter Method.....	33
5.2 SBR values of S_0 images obtained for Skim Milk solution in the Linear Polarimeter Method	34
5.3 Number of pixels detected as edges of DOLP images obtained for Skim Milk in the Rotating Retarder Polarimeter Method.....	35
5.4 Number of pixels detected as edges of S_0 images obtained for Skim Milk in the Rotating Retarder Polarimeter Method.....	36
5.5 SBR values of R_{pol} images obtained for Skim Milk in the Linear Polarimeter Method	41
5.6 Number of pixels detected as edges of R_{pol} images obtained for Skim Milk in the Linear Polarimeter Method	42
5.7 Source Table for DOLP SBR values	46
5.8 Source Table for S_0 SBR values	46

5.9 Source Table for R_{pol} SBR values.....	47
5.10 Source Table for DOLP edges.....	47
5.11 Source Table for S_0 edges.....	48
5.12 Source Table for R_{pol} edges.....	48
5.13 Source Table Comparing Regression Slopes of DOLP and S_0 images (SBRs).....	49
5.14 Source Table Comparing Regression Slopes of DOLP and R_{pol} images (SBRs).....	50
5.15 Source Table Comparing Regression Slopes of DOLP and S_0 images (edges).....	50
5.16 Source Table Comparing Regression Slopes of DOLP and R_{pol} images (Edges).....	51

LIST OF FIGURES

Figure	Page
2.1 Propagation of Linearly polarized light	9
2.2 Propagation of Circularly polarized light	10
3.1 Sketch of the Optical phantom.....	12
3.2 Sketch depicting the Experimental Setup using the Rotating Retarder Polarimeter method.....	13
3.3 Sketch depicting the Experimental Setup using the Linear Polarimeter method.....	14
5.1 DOLP Image of Optical Phantom in 18ml of Water in Test Tube	27
5.2 DOLP Image of Optical Phantom in 18ml of Water+0.2% skim milk solution in Test Tube	27
5.3 DOLP Image of Optical Phantom in 18ml of Water+0.4% skim milk solution in Test Tube	28
5.4 DOLP Image of Optical Phantom in 18ml of Water+0.6% skim milk solution in Test Tube	28
5.5 DOLP Image of Optical Phantom in 18ml of Water+0.8% skim milk solution in Test Tube	29
5.6 DOLP Image of Optical Phantom in 18ml of Water+1.0% skim milk solution in Test Tube	29
5.7 S_0 Image of Optical Phantom in 18ml of Water skim milk solution in Test Tube.....	30
5.8 S_0 Image of Optical Phantom in 18ml of Water+0.2% skim milk solution in Test Tube	30
5.9 S_0 Image of Optical Phantom in 18ml of Water+0.4% skim milk solution in Test Tube	31

5.10 S_0 Image of Optical Phantom in 18ml of Water+0.6% skim milk solution in Test Tube	31
5.11 S_0 Image of Optical Phantom in 18ml of Water+0.8% skim milk solution in Test Tube	32
5.12 S_0 Image of Optical Phantom in 18ml of Water+1.0% skim milk solution in Test Tube	32
5.13 SBR values of <i>DOLP</i> images vs. concentration of volume percentage of skim milk in aqueous solution	34
5.14 SBR values of S_0 images vs. concentration of volume percentage of skim milk in aqueous solution	35
5.15 Number of Pixels detected as edges of <i>DOLP</i> images vs. concentration of volume percentage of skim milk in aqueous solution	37
5.16 Number of Pixels detected as edges of S_0 images vs. concentration of volume percentage of skim milk in aqueous solution	37
5.17 R_{pol} Image of Optical Phantom in 18ml of Water in Test Tube	38
5.18 R_{pol} Image of Optical Phantom in 18ml of Water+0.2% skim milk solution in Test Tube	39
5.19 R_{pol} Image of Optical Phantom in 18ml of Water+0.4% skim milk solution in Test Tube	39
5.20 R_{pol} Image of Optical Phantom in 18ml of Water+0.6% skim milk solution in Test Tube	40
5.21 R_{pol} Image of Optical Phantom in 18ml of Water+0.8% skim milk solution in Test Tube	40
5.22 R_{pol} Image of Optical Phantom in 18ml of Water+1.0% skim milk solution in Test Tube	41
5.23 SBR values of R_{pol} images vs. concentration of volume percentage of skim milk in aqueous solution	43
5.24 Number of pixels detected as edges values for R_{pol} images vs. concentration of volume percentage of skim milk in aqueous solution.....	43

5.25 Comparison of SBR values of DOLP and R_{pol} images vs. concentration of volume percentage of skim milk in aqueous solution	44
5.26 Comparison of number of pixels detected as edges of DOLP and R_{pol} images vs. concentration of volume percentage of skim milk in aqueous solution.....	44

CHAPTER I

INTRODUCTION

1.1 Overview

Identifying different tissue types, abnormalities and numerous types of carcinomas has been the primary objective in tissue diagnostics. Because of its non-ionizing radiation characteristics and its high anatomical and physiological content, optical imaging promises to improve the clinical diagnosis of disease and early tumor detection. Moreover, optical imaging techniques are economical and portable.

Polarization based imaging can reveal hidden objects which would otherwise go unnoticed by conventional imaging techniques. Tissues containing tumors tend to alter the chemical composition, cell physiology, metabolism, density and refractive index, ultimately leading to variations in the optical scattering of light. The optical signatures emitted from the tumors contain metabolic and structural information that contributes to a significant role in polarization based optical imaging [35-41].

Biological tissues are turbid media that have strong scattering and low absorption characteristics in the optical window between deep visible and near infrared NIR (up to

900 nm). Photons undergo three types of scattering when they travel through a turbid medium: 1) snake photons-highly penetrating photons; 2) diffuse photons-highly scattering components, and 3) ballistic photons-weakly scattering components. Upon irradiation of the tissue with polarized light, the diffuse photons lose their initial polarization state while the ballistic photons retain their initial polarization state [43]. Hence, polarimetric imaging is performed by detecting these ballistic photons over the diffuse photons yielding high contrast images.

Giakos [24-29] carried out multi-spectral, multi-fusion polarimetric investigations on targets submerged in turbid biological media. The studies utilized the Rotating Retarder Polarimeter method [30-33] in conjunction with the measurement matrix method [34]. The experiments were successful in providing enhanced image contrast based on refractive index differences as well as in developing new optical contrast agents and biomarkers towards the enhancement of image quality.

1.2 Purpose of Study

Although various techniques using polarized light have been proposed by the researchers for optical imaging of the turbid media, there exists no experimental evidence to show dominance of one technique over the other in describing the characteristics of the tissue.

Recently, Giakos [24-29] advanced the hypothesis that circular polarized waves transmit deeper in scattering media maintaining their polarization characteristics better than the linearly polarized waves. Therefore, he proposed a comparative study aimed to assess the merit of circularly polarized wave-based interrogation of targets over linearly

polarized wave-based interrogation. This study is an attempt to investigate, compare and assess the imaging potential of these two techniques using two different polarimetric geometries to interrogate targets embedded in turbid biological media.

1.3 Objectives of study

The aim of study is to assess the potential of the linear and circular polarization-based tissue interrogation techniques on the image quality of backscattered target detection in turbid media.

1.4 Research Hypotheses

The hypotheses for testing the imaging parameters are presented below. The null hypotheses were tested at a Type-1 error probability of 0.05.

1.4.1 Null hypotheses

- The signal to background ratio (SBR) values for Degree of Linear Polarization (DOLP) and total intensity (S_0) images do not vary with increasing concentration of the scattering agents.
- The SBR values achieved for Degree of Polarization (R_{pol}) images do not vary with increasing concentration of the scattering agents.
- The DOLP images do not have significantly higher SBR values than S_0 images.
- SBR values obtained for DOLP images (circular polarization-based interrogation) are not higher than those of Degree of Polarization (R_{pol}) images (linear polarization-based interrogation).

1.4.2 Alternate hypotheses

- The signal to background ratio (SBR) values for Degree of Linear Polarization (DOLP) and total intensity (S_0) images vary with increasing concentration of the scattering agents.
- The SBR values achieved for Degree of Polarization (R_{pol}) images vary with increasing concentration of the scattering agents.
- The DOLP images have significantly higher SBR values than S_0 images.
- SBR values obtained for DOLP images (circular polarization-based interrogation) are higher than those of Degree of Polarization (R_{pol}) images (linear polarization-based interrogation).

1.5 Limitations of the Study

- a) The experiments were done using a preclinical optical phantom. In vivo studies were not conducted.
- b) The study was performed with only one wavelength (633 nm); expansion of this study in the NIR domain is desirable.

CHAPTER II

LITERATURE REVIEW

2.1 Optical Imaging

Optical imaging presents several potential advantages over existing radiological techniques. The advantages of optical imaging are discussed as follows:

- a) The radiation is non-ionizing, and therefore it is offered for continuous monitoring of disease detection, treatment, and patient follow-up, without the hazards imposed by the ionizing modalities (x-rays, gamma rays etc).
- b) Optical Imaging methods offer the potential to differentiate between soft tissues, due to their different absorption or scattering characteristics at NIR wavelengths providing useful information unavailable to other modalities.
- c) The specific absorption by natural chromophores (such as oxy-hemoglobin) allows functional information to be obtained [1].
- d) It offers for the design of low-cost diagnostic devices.

During the last decade, optical imaging using polarization state of light as a discrimination criterion has been of considerable interest [2-5]. These methods assume that weakly scattered light retains its initial polarization state whereas highly scattered

light does not [6-7]. The scattering events depend on the size, shape, concentration and refractive indices of scatterers [7-8].

Nothdurft et al [9] studied the effectiveness of using polarized illumination and detection to enhance the visibility of targets buried in highly scattering media. The experimental results indicate that target visibility improvement achieved by a specific polarization method depends on both the background optical properties and the target type. It was also stated that, by analyzing all the polarization images, it is possible to reveal certain information about target or the scattering background.

Jacques et al [10] demonstrated that polarization sensitive detection could discriminate different skin pathologies. Results from the study suggest that birefringent dermal collagen randomizes polarized light yielding imaging based on backscattered photons from superficial epidermal and papillary dermis.

Rakovi'c et al [11] presented both experimental and Monte Carlo based simulation results for a diffusely backscattered intensity patterns taken from a turbid media which was illuminated with polarized light. The two dimensional Mueller matrix was calculated and was compared with experimental results involving a turbid medium. The experimental and numerical results were in a good agreement.

Backman et al [12] demonstrated that polarization based imaging can detect epithelial cell dysplasia. Yaroslavsky et al [13] reported a fluorescence method to differentiate cancerous skin cells using linearly polarized light.

Kartazayeva et al [14-15] used a time-resolved technique and imaging to study the different propagation characteristics under linearly and circularly polarized illumination.

Illumination of tissue with linearly polarized light was studied by many researchers. The application of polarizers and ratios involving parallel and perpendicular analyzer positions provided the researchers with enhanced view of vasculature [16-17] and superficial tissue [17-18]. Sudha et al [19] proposed that by illuminating the target with polarized light at two different wavelengths, the visibility of subsurface tissues was increased.

2.2 Polarimetry based optical imaging

Demos et al [2] reported that bulk pathological tissues depolarize incident light photons to a greater extent than normal tissues. They used polarization discrimination of backscattered photons on a one centimeter thick breast chicken tissue. Using a non-Rotating Retarder Polarimeter method, they observed image structures at different depth zones.

Hielscher et al [20] used a Stokes vector–Mueller matrix approach to polarized light scattering. They measured the two dimensional Mueller matrix of a backscattered light from a turbid medium.

Baba et al [21] proposed an automated Mueller matrix polarimetric imaging system for cancer detection. A sixteen element Mueller matrix of the tissue phantom was generated using a horizontal polarizer and diffuser plate as known samples. Nezhuvungal et al [22] reported the use of Mueller matrix based imaging system for tissue diagnostics.

Goudail et al [23] demonstrated a system that measures the polarimetric state of light coming from each point of the phantom. The polarimetric images proved to enhance target detection. A liquid crystal polarization modulator was used to determine the Stokes parameters at each spatial location.

Giakos [24-29] proposed novel multi spectral, multi fusion polarimetric imaging techniques introducing multi wavelength image difference techniques, as well as advanced polarimetric methodologies in combination with optically active molecules. The samples were illuminated with circular polarized light at different wavelengths and by rotating the analyzing retarder, raw images were captured. The images were processed to obtain Stokes parameters (S_0 , S_1 , S_2 , and S_3) of the light backscattered from the sample. A Stokes parameters image difference between acquired images at different wavelengths indicated a significant enhancement of the image contrast. Further improvements were obtained by doping the surrounding background of the target with optically active molecules, such as glucose and amino acids.

2.3 Polarized Light

Light is an electromagnetic wave that propagates in the electric field. The propagation can be explained by Maxwell's equations. These equations predict the velocity of propagation of electromagnetic waves in media which is in close agreement with the measured velocity of light.

$$\nabla \times \mathbf{E} = -\frac{\partial \mathbf{B}}{\partial t} \quad 2.1$$

$$\nabla \times \mathbf{B} = \mu_0 \mathbf{J} + \mu_0 \epsilon_0 \frac{\partial \mathbf{E}}{\partial t} \quad 2.2$$

Where \mathbf{E} and \mathbf{B} are electric and magnetic wave vector fields, respectively, μ_0 (N/A²) & ϵ_0 (F/m) are, respectively, the magnetic permeability and electrical permittivity of vacuum and \mathbf{J} (A/m²) is current density. The direction of this electric field oscillation as it propagates defines the polarization [30].

In general, light is un-polarized i.e. it travels as vibrations in all directions where all planes of propagation being equally probable. Light is said to be linearly polarized when the transverse electric field is in phase with the magnetic field. Based on the amplitudes of these orthogonal components, the direction of the light is decided.

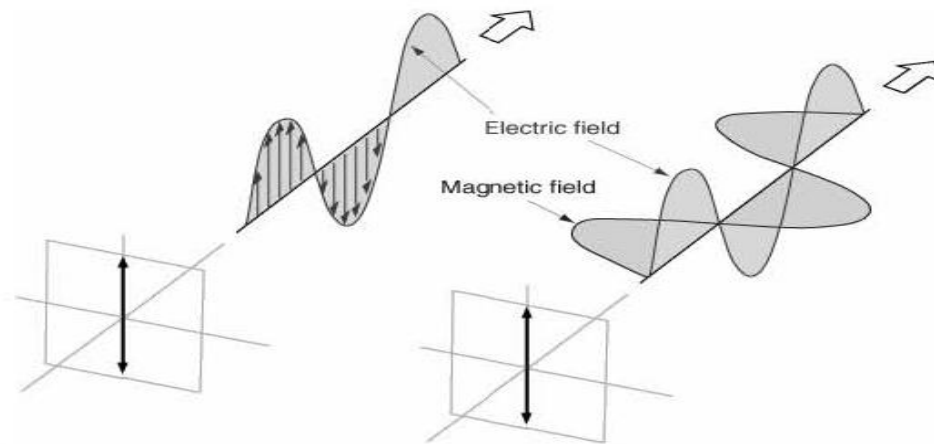


Figure 2.1 Propagation of Linearly polarized light [47]

If light is composed of two plane waves of equal amplitude with a phase difference of 90°, then the light is said to be circularly polarized.

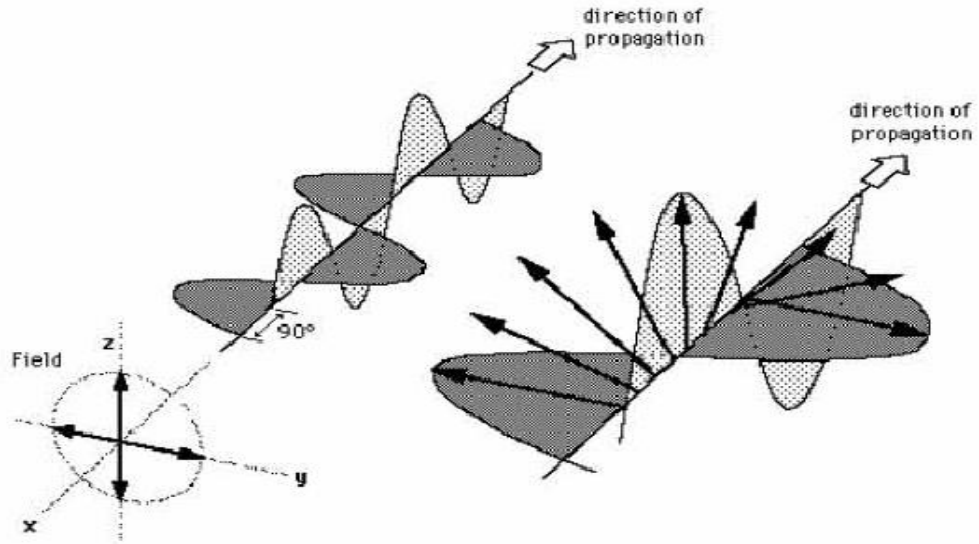


Figure 2.2 Propagation of Circularly polarized light [47]

2.4 Stokes Parameters

The Stokes parameters describe the polarization state of electromagnetic radiation. The change in polarization states of light is caused because of the change in the orientation of the electric vector in time and space. The Stokes parameters are given by

$$S_0 = E_x^2 + E_y^2 \quad (2.3)$$

$$S_1 = E_x^2 - E_y^2 \quad (2.4)$$

$$S_2 = 2E_x E_y \cos \delta \quad (2.5)$$

$$S_3 = 2E_x E_y \sin \delta \quad (2.6)$$

Where E_x and E_y represent the electric field amplitudes [V/cm^2], δ represents the phase difference between orthogonal electric field components.

The first Stokes parameter S_0 describes the total intensity of the optical beam; the second parameter S_1 describes the preponderance of Linear Horizontal Polarized light over Linear Vertical polarized light. The third parameter S_2 describes the preponderance of Linear +45P light over Linear -45P light and, finally; S_3 describes the preponderance of Right Circular Polarized light over Left Circular Polarized light.

2.5 Polarimetric imaging parameters

Using the Stokes parameters, the following polarimetric imaging parameters can be calculated:

$$DOP = \frac{\sqrt{S_1^2 + S_2^2 + S_3^2}}{S_0} \quad 0 \leq DOP \leq 1 \quad (2.7)$$

$$DOLP = \frac{\sqrt{S_1^2 + S_2^2}}{S_0} \quad 0 \leq DOLP \leq 1 \quad (2.8)$$

$$DOCP = \frac{S_3}{S_0} \quad 0 \leq DOCP \leq 1 \quad (2.9)$$

Where DOP is the degree of polarization, DOLP is the degree of linear polarization; DOCP is the degree of circular polarization [42].

CHAPTER III

METHODS AND PROCEDURES

3.1 Design of Phantom

A hollow cylinder made up of polystyrene material immersed into 18 ml water solution as shown in Fig 3.1 was used as the preclinical phantom for the study. The polystyrene cylinder (index of refraction 1.55) was chosen so that to emulate biological structures such as micro calcifications. The inner diameter of the test tube was 25 mm and the length of the test tube was 90 mm. The distance between the surface of the polystyrene cylinder and the wall of the test tube was $1.7\text{mm} \pm 0.5\text{mm}$. The liquid phase solution consisted of skim milk aqueous solution. Skim milk is a Mie scattering medium, with an index of refraction 1.5 and contains predominantly casein ($0.05\text{-}0.3\ \mu\text{m}$) micelles, suitable for simulation of biological tissue studies [24-29]. Skim milk acts as a scattering agent which replicates the scattering properties of biological tissues.

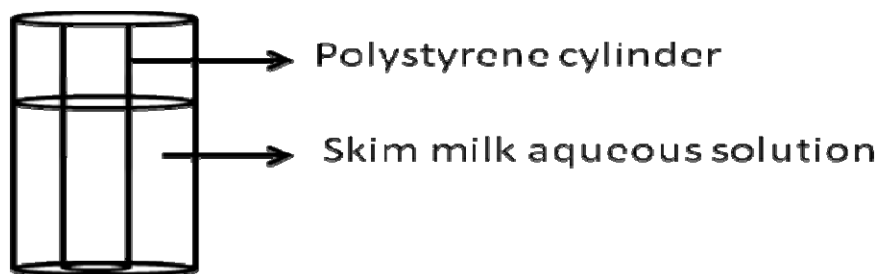


Figure 3.1 Sketch of the Optical phantom

3.2 Experimental Setup

Two sets of experiments were performed in the study. The first set of experiments involved the Rotating Retarder Polarimeter Method [30-33] in conjunction to the Measurement Matrix Method [34] and the studies were conducted with the visible laser source using a setup aligned in backscattered geometry as shown in Fig 3.2. A visible laser source of 633nm was used along with a neutral density filter to reduce the intensity of laser beam. Since the main interest of this experiment was to compare two techniques a visible laser was chosen. A beam expander was used to distribute the light uniformly over the desired area. To achieve the circular polarization, two linear polarizers in conjunction with quarter wave retarders were used. A CCD camera was used to acquire the backscattered intensities from the phantom. The images were later processed on a computer using V++ software.

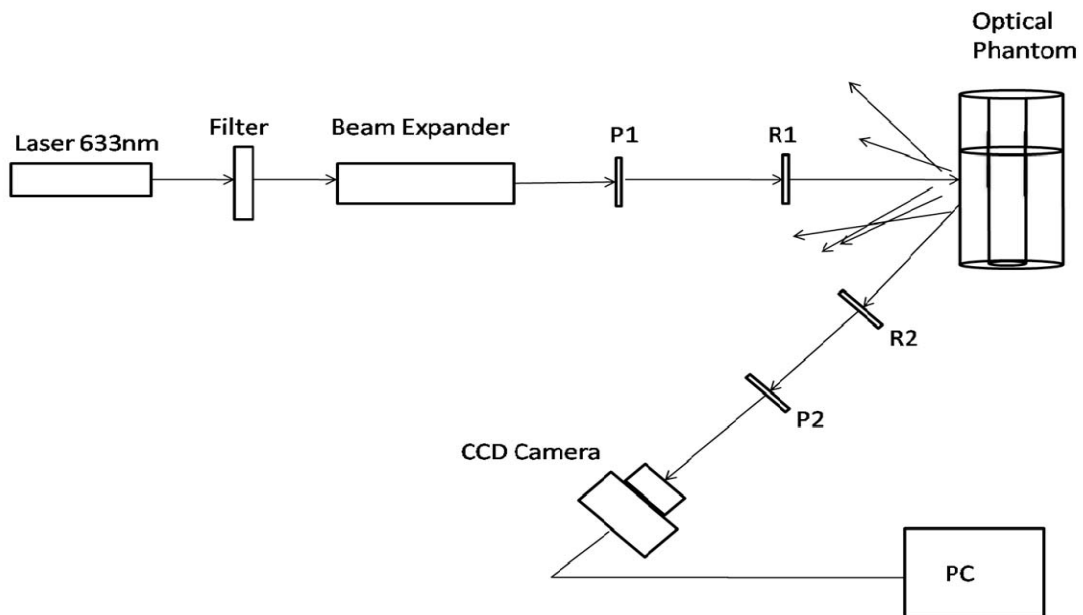


Figure 3.2 Sketch depicting the Experimental Setup using the Rotating Retarder Polarimeter method

The second set of experiments involved the Linear Polarimeter Experimental Setup and the studies were conducted with the visible laser source using a setup aligned in backscattered geometry as shown in Fig 3.4. A visible laser source of 633nm was used along with a neutral density filter to reduce the intensity of laser beam. A beam expander was used to distribute the light uniformly over the desired area. To achieve the linear polarization, two linear polarizers were used. A CCD camera was used to acquire the backscattered intensities from the phantom. The images were later processed on a computer using V++ software.

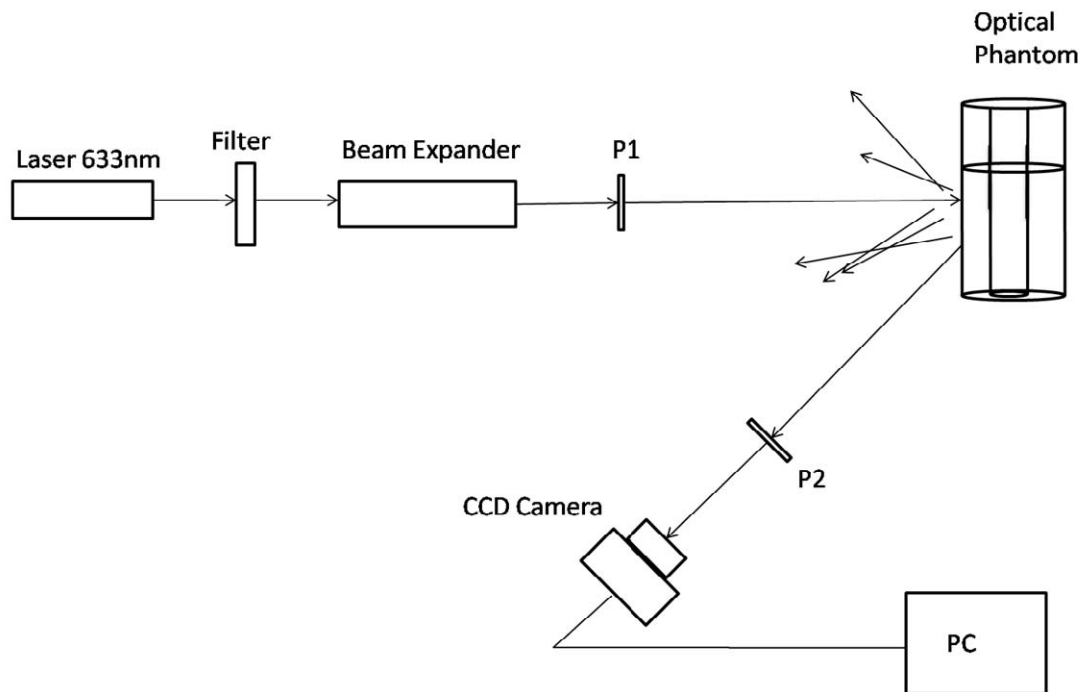


Figure 3.3 Sketch depicting the Experimental Setup using the Linear Polarimeter method

3.3 Experimental Procedures

The experimental procedures involved with both the polarization techniques are discussed here. Skim milk solution was used as a scattering agent in both of the experimental setups.

3.3.1 The Rotating Retarder Polarimeter Experimental Setup

The setup shown in Fig 3.2 was used to investigate the target with circularly polarized light. This setup is commonly called the Rotating retarder Polarimeter method [33-34]. This setup has a transmission side and an analyser side.

Once the experiment was setup according to this geometry, laser light from the 633nm visible laser source was passed through the filter, beam expander and the linear polarizer P1 from which the emerging linearly polarized light passed through a retarder R1. The retarder was used to convert linearly polarized light to circular polarized light before hitting the target. This constituted the transmission side of the setup.

Once the light illuminated the target, the backscattered light was passed through a retarder R2 which converts the circularly polarized light back to linearly polarized light. This retarder R2 was rotated through 0-180° with an angular increment of 22.5° to obtain eight images at different polarization states. The light beam then was passed through a linear polarizer P2 onto the CCD camera. The CCD camera acquired images for every rotation made by the retarder R2 and once all the images were obtained, the Stokes parameters, the Degree of Linear Polarization (DOLP) images and the total intensity S_0

images were obtained with the help of a PC. This constituted the analyzer side of the setup.

The phantom contained 18ml of water to which skim milk was added in volume percentage increments of 0.2%. For each concentration of the skim milk solution, eight images were taken by rotating the retarder from 0° to 180° in steps of 22.5° . The images were then processed to compute the Stokes parameters and thereby the DOLP images were attained.

3.3.2 The Linear Polarimeter Experimental Setup

The setup shown in Fig 3.4 was used to investigate the target with linear polarized light. This setup also has a transmission side and an analyser side.

Once the experiment was setup according to this geometry, laser light from the 633nm visible laser source was passed through the filter, beam expander and the linear polarizer P1. A polarizer was used to convert the light to a linearly polarized light before hitting the phantom. This constituted the transmission side of the setup. Once the light illuminated the target, the backscattered light was passed through a linear polarizer P2 onto the CCD camera. This constituted the analyser side of the setup.

The phantom contained 18ml of water to which skim milk was added in volume percentage increments of 0.2%. The images were then acquired by setting the analyzing polarizer P2 both parallel and perpendicular to the generating polarizer P1 to obtain co-polarized (I_{par}) and cross-polarized (I_{per}) images respectively. The images once obtained,

were stored and processed by using a PC to obtain the Degree of Polarization (R_{pol}) images.

3.4 Alignment and Calibration Procedures

Calibration and alignment are of utmost importance in any optical imaging experiment. To avoid any measurement errors during the study, the system should be aligned first. Polarizers and the retarders were mounted and calibrated before aligning the setup for experimental procedures [45]. The following section presents a description of the alignment procedures.

The alignment of the setup for the Linear Polarimeter method was similar to the Rotating Retarder Polarimeter method except that the retarders were not present in the former case. Hence, the system was first aligned according to the Rotating Retarder Polarimeter method and then tested for both the methods. The alignment of the optics was done starting with the transmission side. First, the laser source and the phantom were mounted on the optical tabletop. The beam expander was mounted in front of the laser source for uniform distribution of light on the phantom. The neutral density filters were then mounted in between the laser source and beam expander to obtain the desired illumination of the target. The polarizer P1 was placed in front of the beam expander with a maximum orientation. The retarder R1 oriented at 45° was placed in between the polarizer P1 and the phantom to produce circularly polarized light.

The alignment on the analyzer side was done by placing the CCD camera in a backscattered geometry at a working distance of 20cm from the Optical Phantom. The retarder R2 oriented at 0° was placed in between the phantom and the CCD camera. The

polarizer P2 whose orientation was parallel to the polarizer P1 was mounted in between the retarder R2 and the CCD camera.

Once the alignment was achieved, the setup was tested for high image resolution and beam optimization. The phantom was replaced by a white paper and eight intensity contributions were recorded by the Rotating Retarder Polarimeter method from which the Degree of Linear Polarization (DOLP) and total intensity (S_0) images were obtained. The resulting images made sure that uniform illumination was achieved in the process. The white paper was then removed and was replaced again with the phantom.

3.5 Image Processing

The contrast values were computed and edge detection techniques (Sobel algorithm) were used to assess the quality of an image. The signal to background ratio value was used as a measure of contrast. A Sobel filter was used to calculate the number of pixels registered as edges in an image [46]. The Sobel edge detection was used as due to its simplicity and it gives the orientation of the edges detected.

Experiments involving the Rotating Retarder Polarimeter method yielded a set of eight images containing polarimetric information of the phantom. These images were processed in MATLAB using a program yielding S_0 and DOLP images. Giakos [7] proposed that the Signal-to-Background Ratio (SBR) values can be computed for an image given by

$$SBR = \frac{S - B}{\frac{1}{2}(S + B)} \quad (3.1)$$

Where S represents the average intensity of the selected pixels in the signal and B represents the average intensity of the selected pixels in the background. The SBR values range between zero and two. The Signal-to-Background Ratio (SBR) values were then computed for the S_0 and DOLP images.

The mean intensities of the signal and background were calculated after removing the outliers by calculating the inter quartile range. The number of pixels registered as edges for the S_0 and DOLP images was then computed in MATLAB. Thus for every increment in concentration of milk added, the signal to background ratio values and number of pixels registered as edges for S_0 and DOLP images were computed.

Experiments involving the linear Polarimeter setup yielded co-polarized (I_{par}) and cross-polarized (I_{per}) images respectively. The acquired images were then processed to obtain the Degree of Polarization given by

$$R_{pol} = \frac{I_{par} - I_{per}}{I_{par} + I_{per}} \quad (3.2)$$

Where I_{par} and I_{per} are co-polarized and cross-polarized detected light intensities respectively. Thus for every increment in concentration of milk added, the signal to background ratios and number of pixels registered as edges of R_{pol} images were computed.

3.6 Analysis Techniques

The statistical analysis was performed on the DOLP, S_0 and R_{pol} images based on the null hypotheses discussed in chapter 1.4.1. The mean intensity values of signal and

background were calculated after removing the outliers using Adobe Photoshop environment. Removal of outliers eliminated any noise present due to reflections.

The DOLP and S_0 images obtained from the Rotating Retarder Polarimeter setup and the R_{pol} images obtained from the Linear Polarimeter setup were processed to obtain SBR values. Edge detection was also done on the images to determine the number of pixels registered as edges that contain important structural information. Sobel edge detection technique was used to calculate the number of pixels registered as edges in DOLP, S_0 and R_{pol} images.

The null hypotheses was tested by performing Model-I Linear Regression Analysis with a type-1 error probability of 0.05 and the Regression Equation was given by

$$\hat{Y} = \alpha + \beta X \quad (3.3)$$

Where \hat{Y} represents the predicted value of dependant variable and X represents the value of independent variable.

The experiments were repeated three times to check for the repeatability and reproducibility of the results. Once all the computations were performed and the desired images were obtained, statistical analysis was performed on the data to test the hypotheses. Comparison of the regression lines was also done to test the equality of slopes obtained on the data collected in the experiments.

CHAPTER IV
MATERIALS USED

4.1 Optical Table Top

To avoid inconsistent measurements and misalignment an optical table top from Melles Griot (Carlsbad, CA) was used to mount the optical components.

4.2 Laser Source

A 633nm semiconductor, Red, Uniphase Helium – Neon Laser (JDS 1135P Uniphase Red He-Ne Laser) source was used to illuminate the target and its specifications are presented in Table 4.1.

Table 4.1 Specifications of Laser Source

Wavelength	633nm
Minimum Output Power	10mW
Beam Diameter	0.68mm
Beam Divergence	1.2mrad
Operating Voltage	3100 V DC
Operating Current	6.5 mA
Maximum Noise	1 %

4.3 Neutral Density Filter

To reduce the intensity of laser light, a 25mm diameter neutral density filter (Coherent Inc., Auburn, CA) was used in the study.

4.4 Linear Polarizers

Two dichroic sheet high contrast polarizers (03 FPG 001, Melles Griot, Rochester, NY) were used, one on the transmission side and the other on the receiver side. The polarizers were made of plastic dichroic polarizing sheet sandwiched between strain free glass plates. Specifications of the polarizers are presented in Table 4.2.

Table 4.2 Specifications of the Polarizers

Wavelength Range	350-650nm
Optic Material	Plastic dichroic polarizing sheet
Transmission	32%
Diameter	20.6 +/- 0.25 mm
Thickness	2.6 +/- 0.2 mm
Acceptance Angle	$\pm 20.6^\circ$
Operating Temperature	-20°C to +120°C

4.5 Quarter wave Retarders

Two retarders were used, one on the transmission side and the other on the analyzer side, the details of which are presented below.

4.5.1 Berek Polarization Compensator

The Berek compensator is a variable wave plate which can be used as a quarter wave plate or a half wave plate. It works in the wavelengths ranging between 200nm to 1600nm. It was used on the transmission side as a quarter wave plate to achieve the circular polarization. The specifications of the 5540 Berek polarization compensator are as shown in Table 4.3.

Table 4.3 Specifications of the Berek compensator

Wavelength Range	200–1600 nm
Aperture	12 mm
Wavefront Distortion	<1/8 wave
Retardance	0-5.8 π @300nm 0- π @1600nm
Resolution	0.001 wave @ null 0.01 wave @ 2 π

4.5.2 Quartz Quarter Wave Retarder

A quartz quarter wave plate (02 WRQ 007, Melles Griot, Carlsbad, CA) used was used as a rotating retarder on the analyzer side of the experimental setup. The specifications of the Quartz Quarter Wave Retarder are as presented in Table 4.4.

Table 4.4 Specifications of the Quarter wave Retarder

Wavelength Range	193-2300nm
Material	Crystal Quartz, c-axis cut
Thickness	2.0mm max
Diameter	20 +0 / -0.15mm
Net Retardance	< 0.01nm/deg.

4.6 Beam expander

To illuminate the phantom uniformly, a beam expander (NT55-579, Edmund Optics Inc., Barrington, NJ) was used that magnifies the laser light to a desired area. The beam expander has a magnification zoom of 50X. The specifications of the beam expander are presented in Table 4.5.

Table 4.5 Specifications of the Beam Expander

Material	Black Anodized Aluminum
Beam Expansion Power	10X-20X
Focus Range	1.2m to ∞
Entrance Aperture	2.0mm maximum
Exit Aperture	34mm maximum

4.7 CCD Camera

A high resolution Photometric Sensys (1401E, Roper Scientific Inc.,) CCD camera system was used to acquire the images of the phantom the specifications of the which, are presented in Table 4.6.

Table 4.6 Specifications of the CCD camera

CCD Image sensor	Kodak KAD1401E
CCD Format	1317 x 1035 imaging pixels plus 26/5 serial pre/post scan pixels; 6.8x6.8 (10-6m)pixel
Frame readout	1.39 seconds per full frame
Readout bits/speed	12 bits @ 1.4 MHz
Operating environment	0 to 40 Deg. Celsius

CHAPTER V

RESULTS AND DISCUSSIONS

In this chapter, experimental results obtained using the Rotating Retarder Polarimeter method and the Linear Polarimeter methods are discussed.

Once the images were obtained, the signal to background ratio (SBR) values and number of pixels registered as edges for DOLP, S_0 and R_{pol} images were calculated. Regions of interest (ROI) for both signal and background areas were chosen for which mean intensities were computed and the statistical analysis were performed after the removal of outliers.

5.1 Results of the Rotating Retarder Polarimeter method

The target (polystyrene cylinder) with 18ml of water was imaged and initial results were recorded on to a PC. Skim milk solution of 0.2% by volume was added in increments of 0.2% to the water solution and the images were acquired for 0.2%, 0.4%, 0.6%, 0.8%, and 1.0% milk solutions. For every increment of skim milk solution, DOLP and S_0 images were obtained. DOLP images obtained from this experiment are presented in Figs 5.1 through 5.6. The DOLP image obtained with 18ml of water is shown in Fig 5.1 and the Figs 5.2 to 5.6 represent the DOLP images obtained when skim milk was

added in volume percentages of 0.2%, 0.4%, 0.6%, 0.8%, and 1.0% to the test tube. The corresponding S_0 images are shown in Fig 5.7 through Fig 5.12.

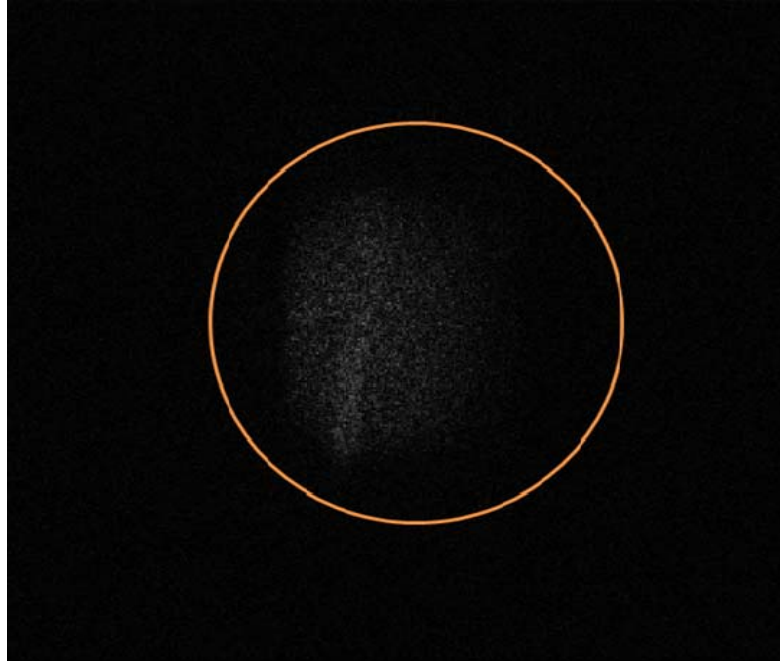


Figure 5.1 DOLP Image of Optical Phantom in 18ml of Water in Test Tube

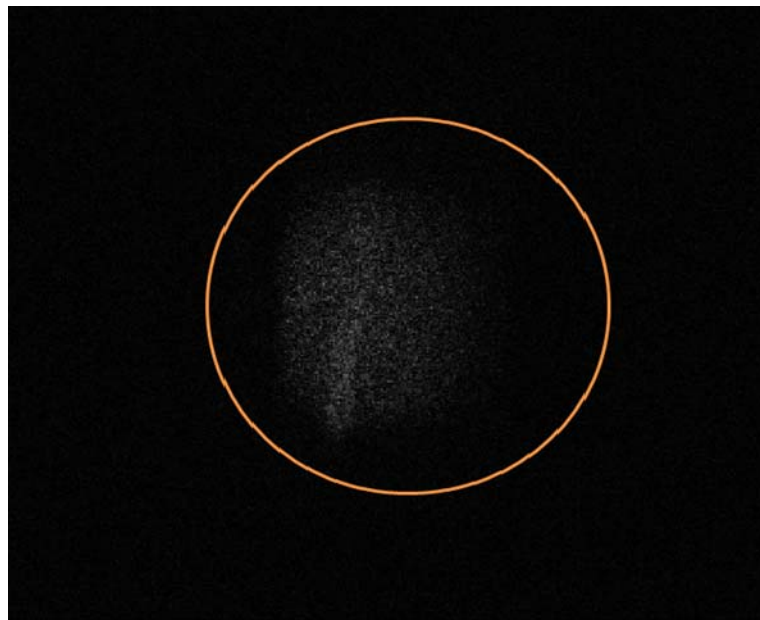


Figure 5.2 DOLP Image of Optical Phantom in 18ml of Water+0.2% skim milk solution
in Test Tube

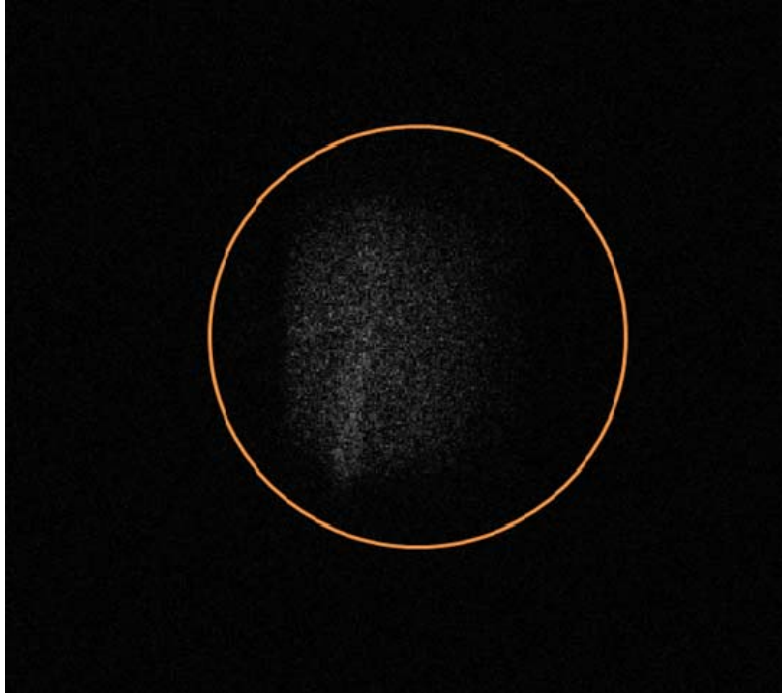


Figure 5.3 DOLP Image of Optical Phantom in 18ml of Water+0.4% skim milk solution
in Test Tube

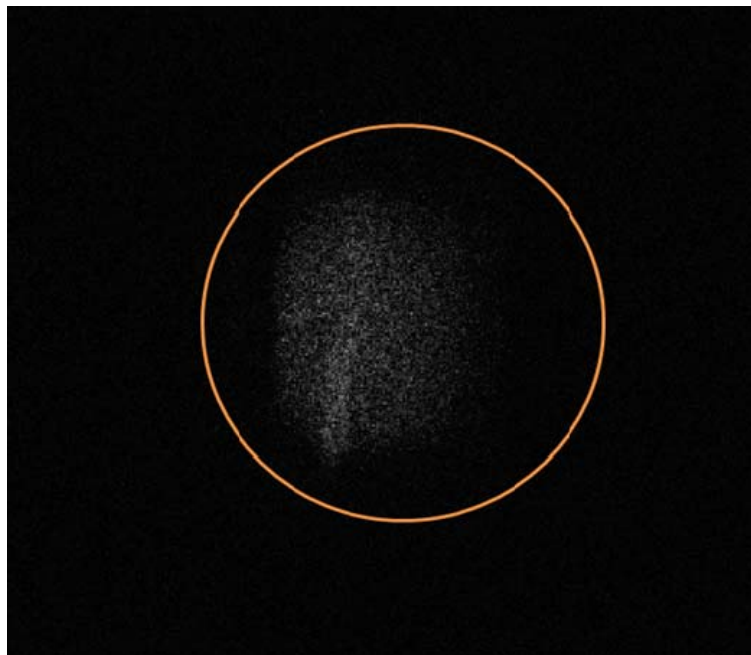


Figure 5.4 DOLP Image of Optical Phantom in 18ml of Water+0.6% skim milk solution
in Test Tube

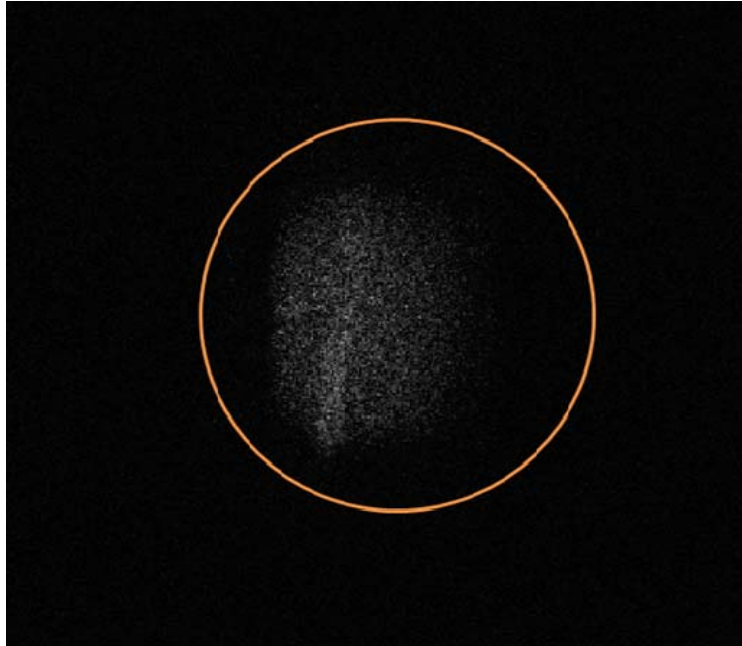


Figure 5.5 DOLP Image of Optical Phantom in 18ml of Water+0.8% skim milk solution
in Test Tube

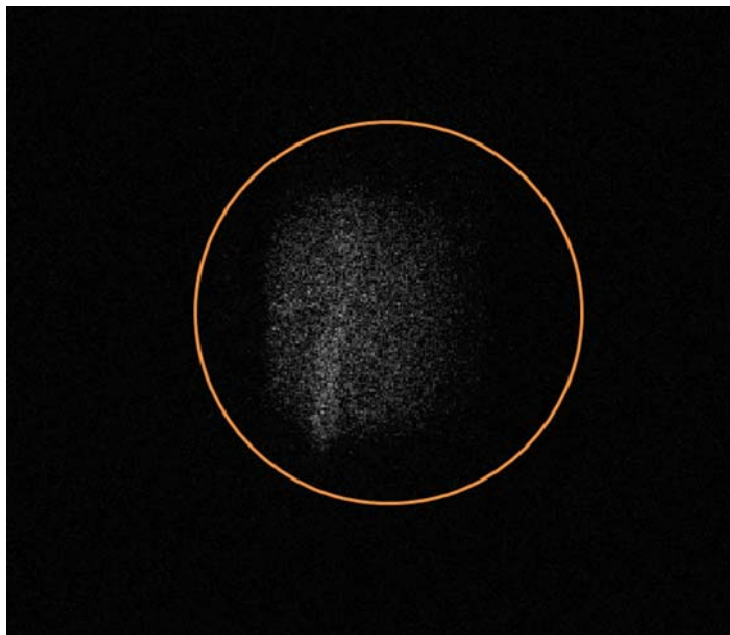


Figure 5.6 DOLP Image of Optical Phantom in 18ml of Water+1.0% skim milk solution
in Test Tube

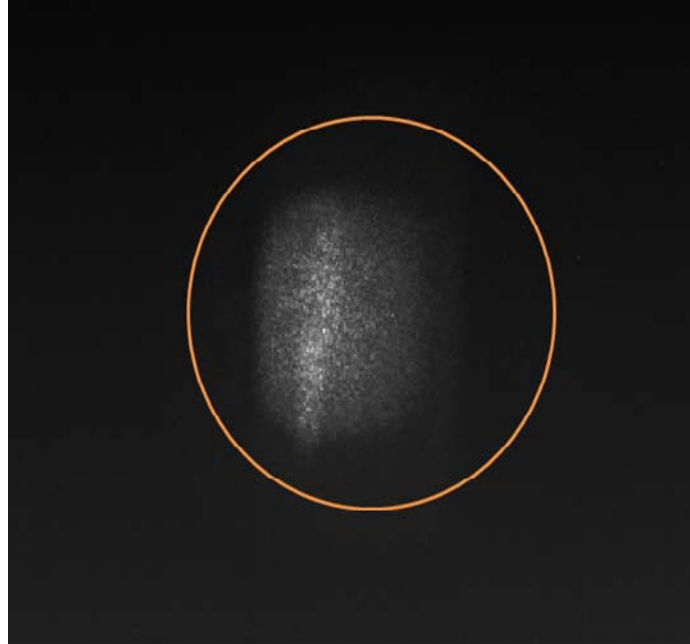


Figure 5.7 S_0 Image of Optical Phantom in 18ml of Water skim milk solution in Test Tube

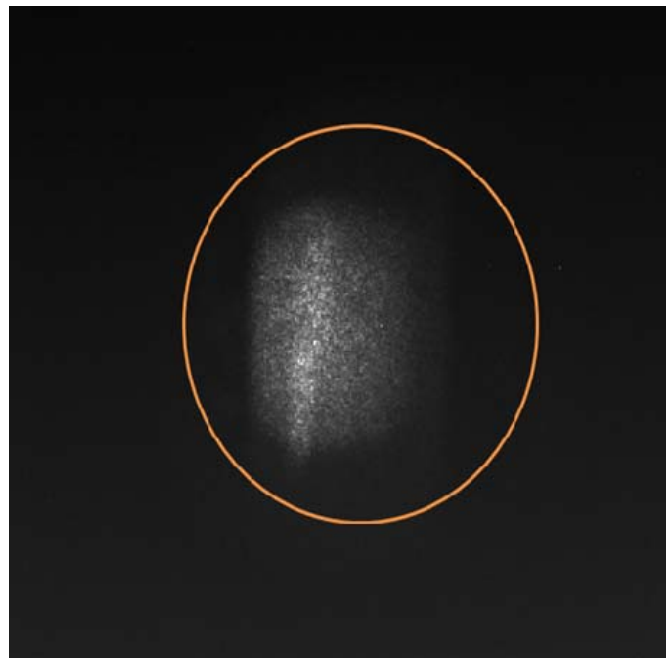


Figure 5.8 S_0 Image of Optical Phantom in 18ml of Water+0.2% skim milk solution in Test Tube

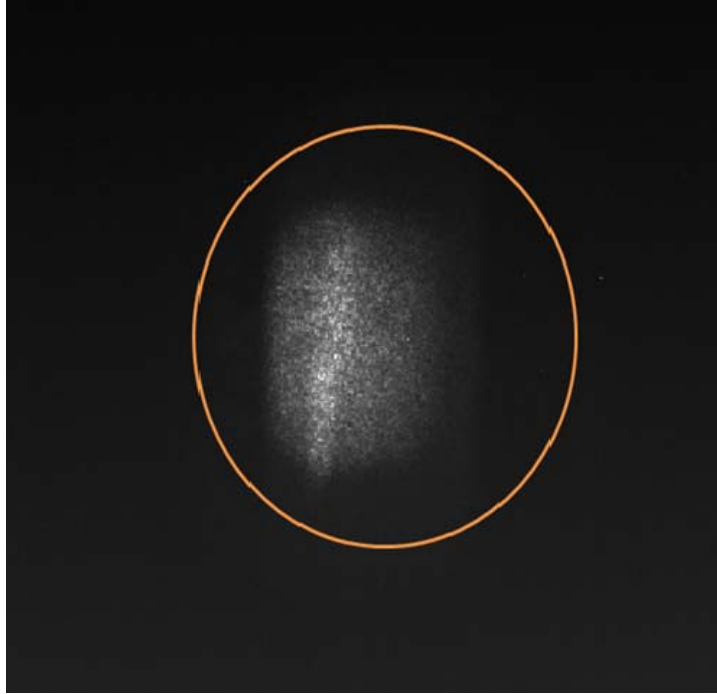


Figure 5.9 S_0 Image of Optical Phantom in 18ml of Water+0.4% skim milk solution in
Test Tube

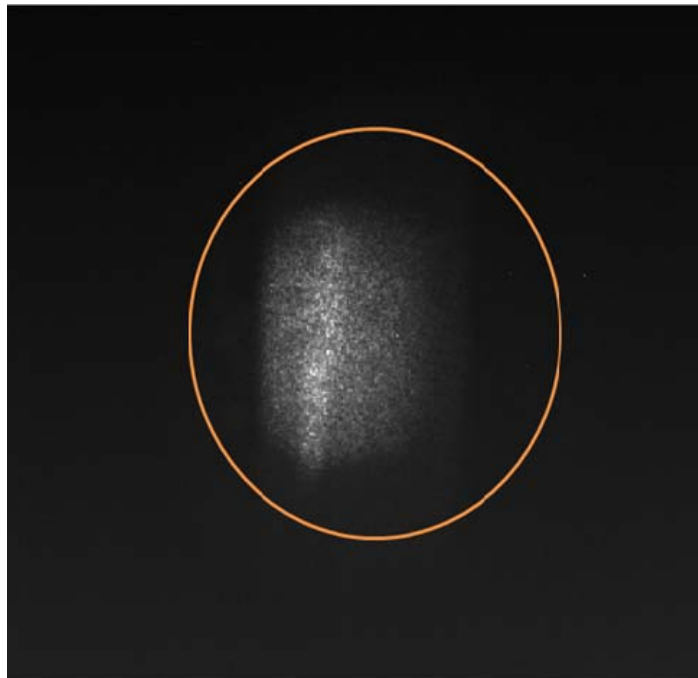


Figure 5.10 S_0 Image of Optical Phantom in 18ml of Water+0.6% skim milk solution in
Test Tube

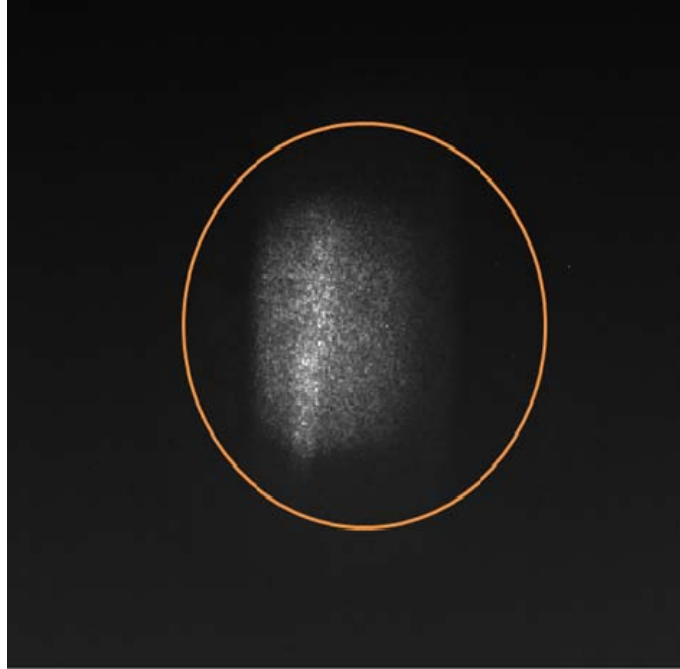


Figure 5.11 S_0 Image of Optical Phantom in 18ml of Water+0.8% skim milk solution in
Test Tube

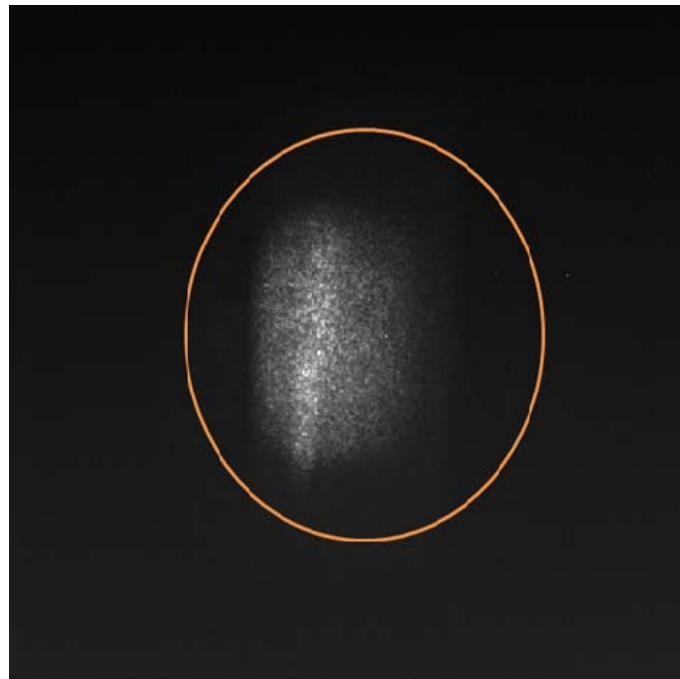


Figure 5.12 S_0 Image of Optical Phantom in 18ml of Water+1.0% skim milk solution in
Test Tube

The Signal to background ratio (SBR) values were calculated for both the DOLP and S_0 images after removing the outliers and calculating the mean intensities from the regions of interest. The computed SBR values for DOLP and S_0 images along with the concentrations of skim milk solution are shown in Table 5.1 and 5.2 respectively.

The plots of SBR vs. volume percentage of skim milk in aqueous solution for DOLP and S_0 images are shown in Fig 5.13 and 5.14 respectively. The figures and plots exhibit an increase in contrast with increasing concentration of skim milk solution.

Table 5.1 SBR values of DOLP images obtained for Skim Milk solution in the Rotating Retarder Polarimeter Method

Concentration [vol %]	SBR
0.0	1.061
0.2	1.402
0.4	1.586
0.6	1.737
0.8	1.856
1.0	1.902

Table 5.2 SBR values of S_0 images obtained for Skim Milk solution in the Rotating Retarder Polarimeter Method

Concentration [vol %]	SBR
0.0	0.501
0.2	0.522
0.4	0.534
0.6	0.547
0.8	0.554
1.0	0.563

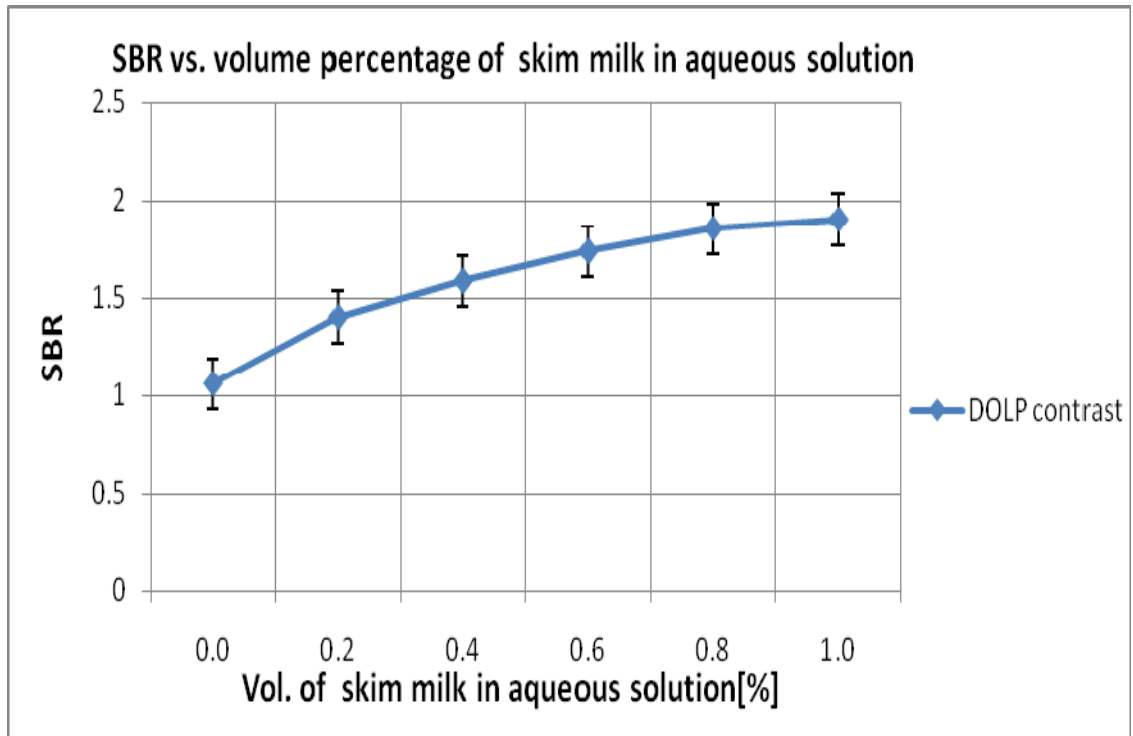


Figure 5.13 SBR values of *DOLP* images vs. concentration of volume percentage of skim milk in aqueous solution

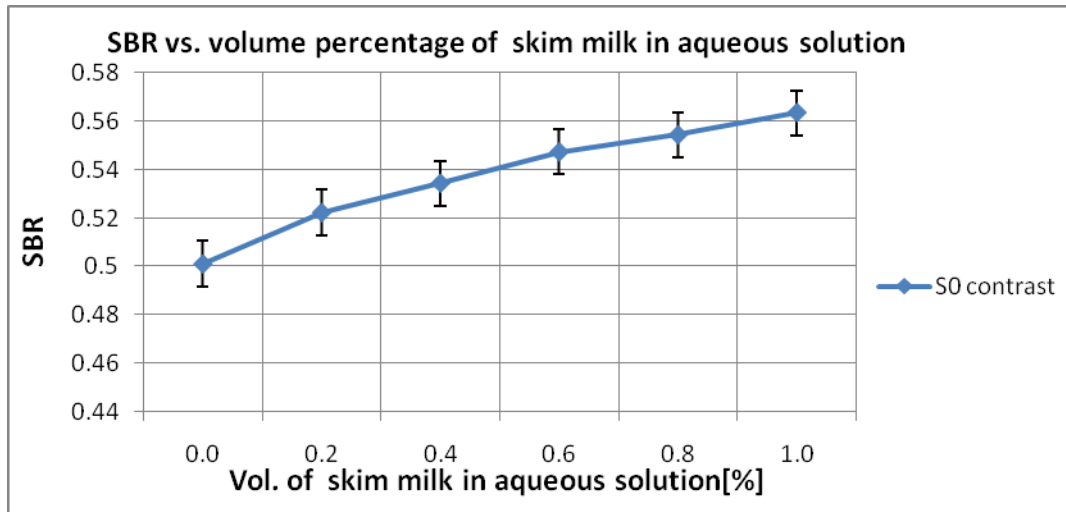


Figure 5.14 SBR values of S_0 images vs. concentration of volume percentage of skim milk in aqueous solution

The number of pixels detected as edges was determined for both the DOLP and S_0 images using the Sobel filter from the regions of interest. The threshold values for the Sobel operator were obtained using the images for water only. The threshold values for DOLP and S_0 images were obtained as 0.0053 and 0.0180 respectively. The computed number of pixels those were detected as edges for DOLP and S_0 images along with the concentrations of skim milk solution is shown in Tables 5.3 and 5.4 respectively.

Table 5.3 Number of pixels detected as edges of DOLP images obtained for Skim Milk in the Rotating Retarder Polarimeter Method

Concentration [vol %]	Number of pixels detected as edges
0.0	4474
0.2	4605
0.4	4660

Table 5.3 Number of pixels detected as edges of DOLP images obtained for Skim Milk in the Rotating Retarder Polarimeter Method (Continued)

0.6	4709
0.8	4765
1.0	4818

The plots of Number of pixels detected as edges vs. volume percentage of skim milk in aqueous solution for DOLP and S_0 images are shown in Fig 5.15 and 5.16 respectively.

Table 5.4 Number of pixels detected as edges of S_0 images obtained for Skim Milk in the Rotating Retarder Polarimeter Method

Concentration [vol %]	Number of pixels detected as edges
0.0	3676
0.2	3749
0.4	3780
0.6	3813
0.8	3839
1.0	3871

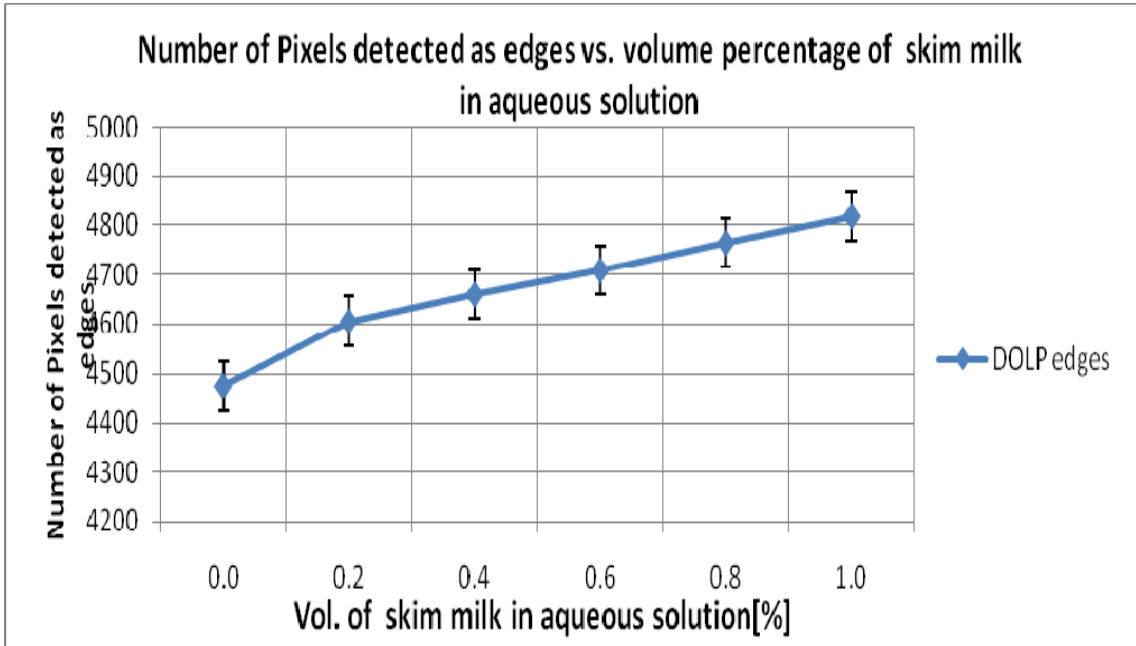


Figure 5.15 Number of Pixels detected as edges of *DOLP* images vs. concentration of volume percentage of skim milk in aqueous solution

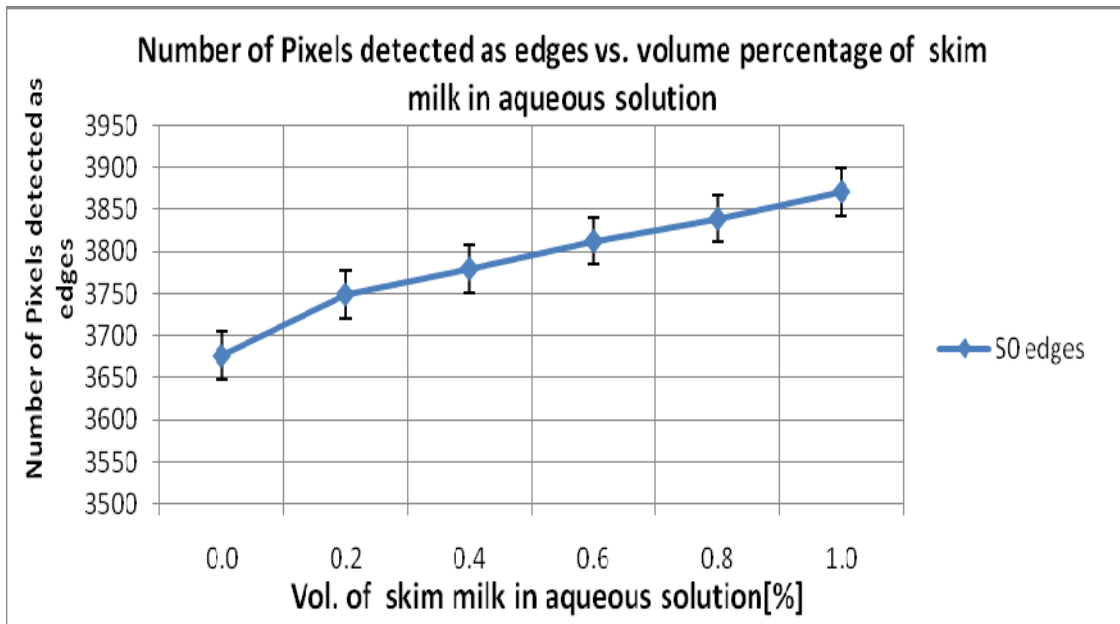


Figure 5.16 Number of Pixels detected as edges of S_0 images vs. concentration of volume percentage of skim milk in aqueous solution

It can be seen that the figures and plots exhibit an increase in number of edges with increasing concentration of skim milk solution.

5.2 Results of the Linear Polarimeter Method

The phantom (target immersed in 18ml of water) was imaged using the CCD camera and the results were recorded onto a PC. Skim milk solution 0.2% by volume was added in increments of 0.2% from 0 to 1.0% thus constituting about 0.2%, 0.4%, 0.6%, 0.8%, and 1.0% of the aqueous solution in five steps. For every increment of skim milk solution, R_{pol} images were obtained. R_{pol} images obtained from this experiment are presented in Fig 5.17 through 5.22.

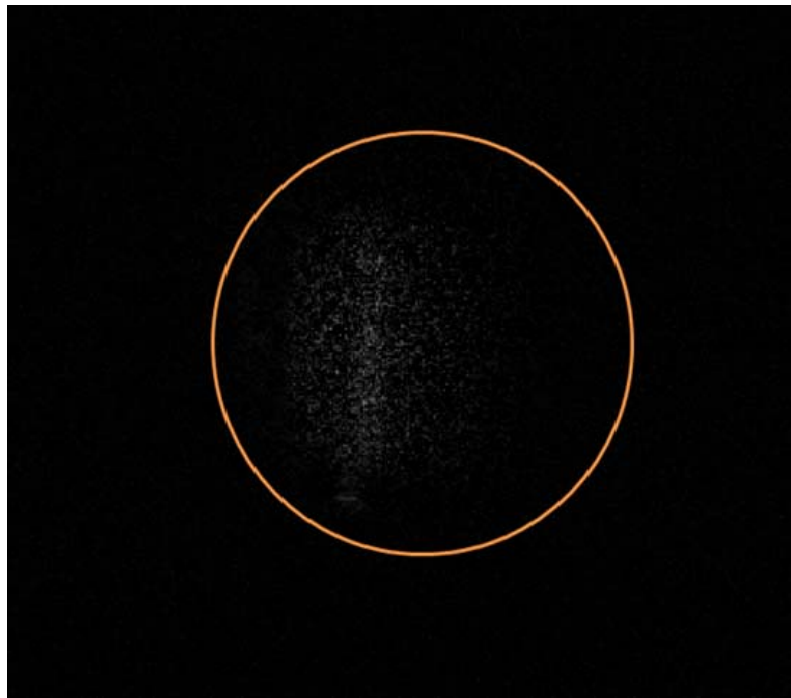


Figure 5.17 R_{pol} Image of Optical Phantom in 18ml of Water in Test Tube

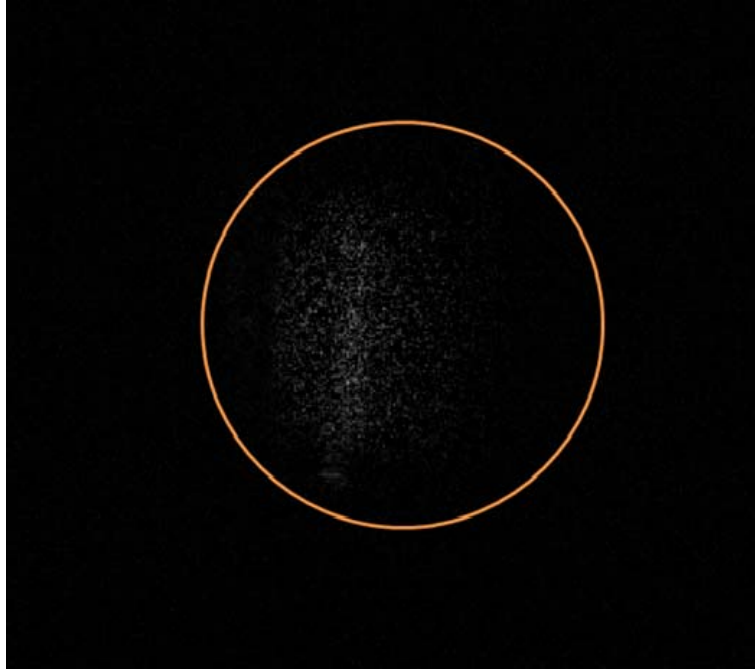


Figure 5.18 R_{pol} Image of Optical Phantom in 18ml of Water+0.2% skim milk solution in Test Tube

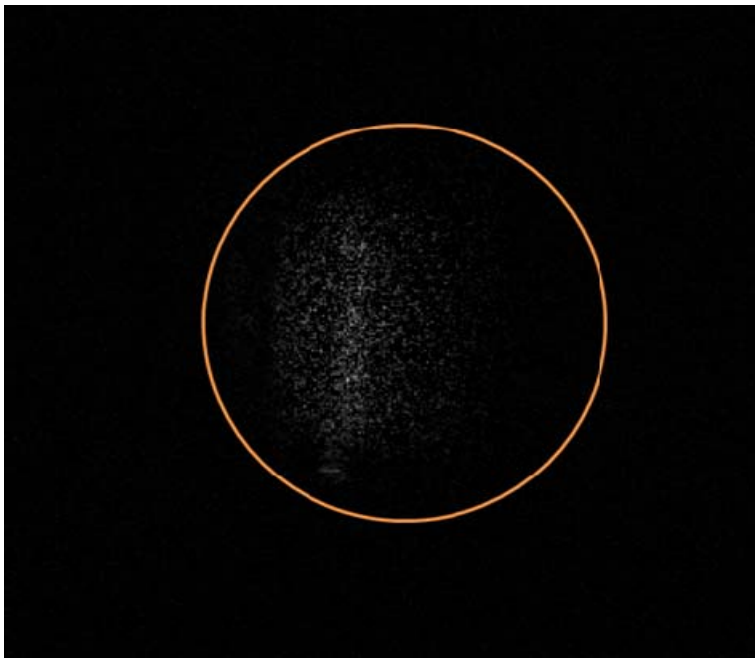


Figure 5.19 R_{pol} Image of Optical Phantom in 18ml of Water+0.4% skim milk solution in Test Tube

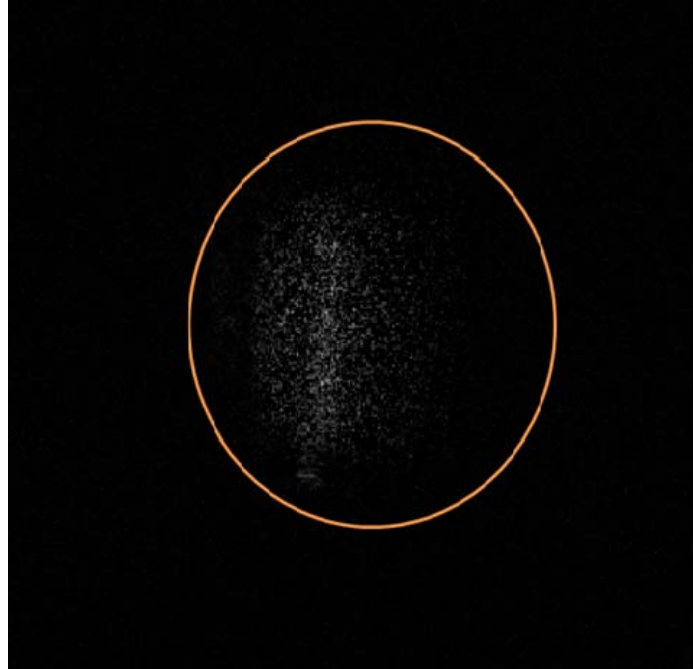


Figure 5.20 R_{pol} Image of Optical Phantom in 18ml of Water+0.6% skim milk solution in
Test Tube

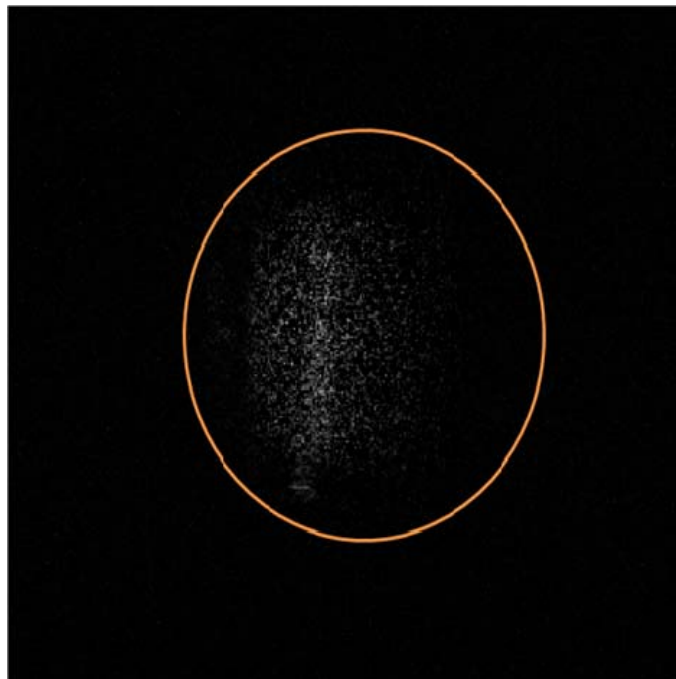


Figure 5.21 R_{pol} Image of Optical Phantom in 18ml of Water+0.8% skim milk solution in
Test Tube

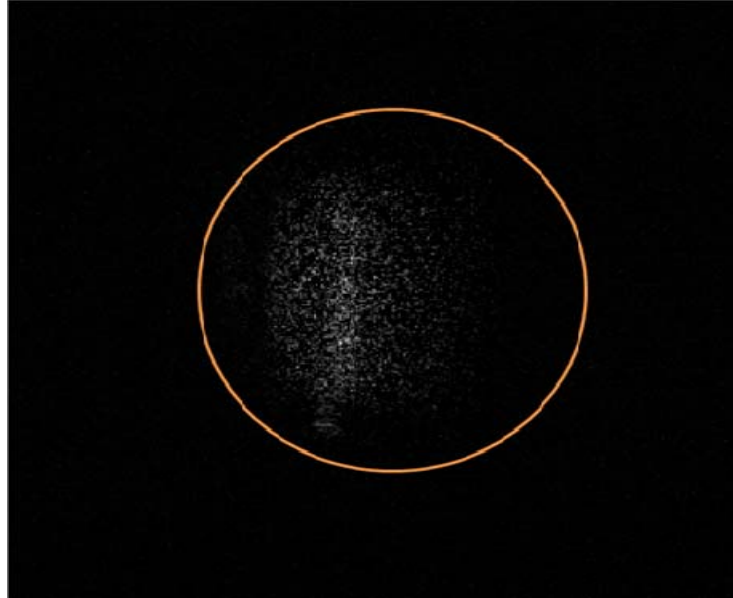


Figure 5.22 R_{pol} Image of Optical Phantom in 18ml of Water+1.0% skim milk solution in Test Tube

The Signal to background ratio (SBR) values was calculated for R_{pol} images after removing the outliers and calculating the mean intensities from the region of interest. The computed SBR values for R_{pol} images along with the concentrations of skim milk solution are shown in Table 5.5. The plot of SBR vs. volume percentage of skim milk in aqueous solution for R_{pol} images are shown in Fig 5.23. The figures and plots exhibit an increase in contrast with increasing concentration of skim milk solution.

Table 5.5 SBR values of R_{pol} images obtained for Skim Milk in the Linear Polarimeter Method

Concentration [vol %]	SBR
0.0	1.010
0.2	1.222
0.4	1.342

Table 5.5 SBR values of R_{pol} images obtained for Skim Milk in the Linear Polarimeter Method (Continued)

0.6	1.447
0.8	1.567
1.0	1.621

The number of edges was calculated for R_{pol} images using the Sobel filter from the region of interest by setting the threshold values. The threshold values were obtained with the phantom in water only as 0.0065. The computed number of pixels detected as edges for R_{pol} images along with the concentrations of skim milk solution are presented in Table 5.6.

Table 5.6 Number of pixels detected as edges of R_{pol} images obtained for Skim Milk in the Linear Polarimeter Method

Concentration [vol %]	Number of pixels detected as edges
0.0	4315
0.2	4473
0.4	4525
0.6	4593
0.8	4655
1.0	4716

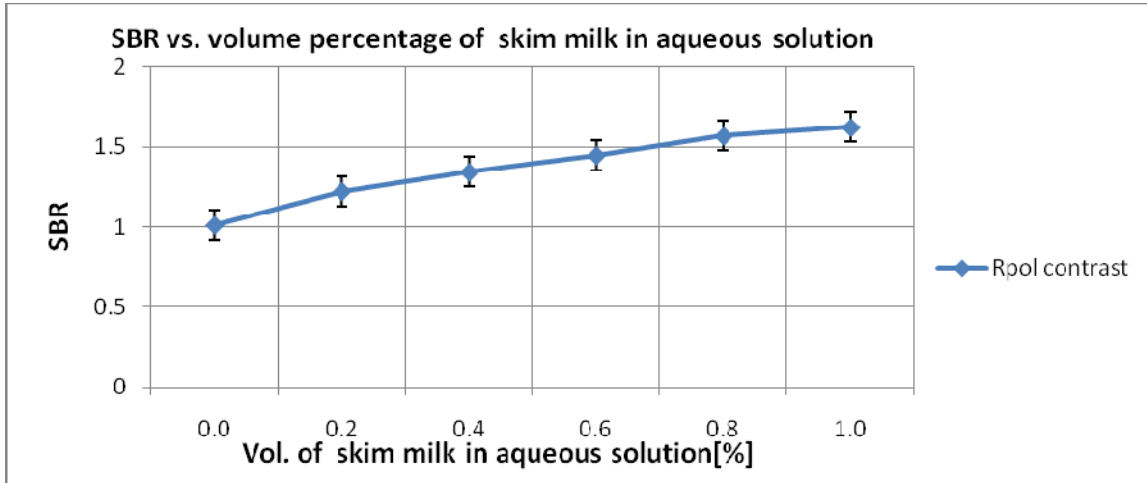


Figure 5.23 SBR values of R_{pol} images vs. concentration of volume percentage of skim milk in aqueous solution

The plot of SBR vs. volume percentage of skim milk in aqueous solution for R_{pol} images are shown in Fig 5.24. It can be seen that the figures and plots exhibit an increase in number of edges with increasing concentration of skim milk solution.

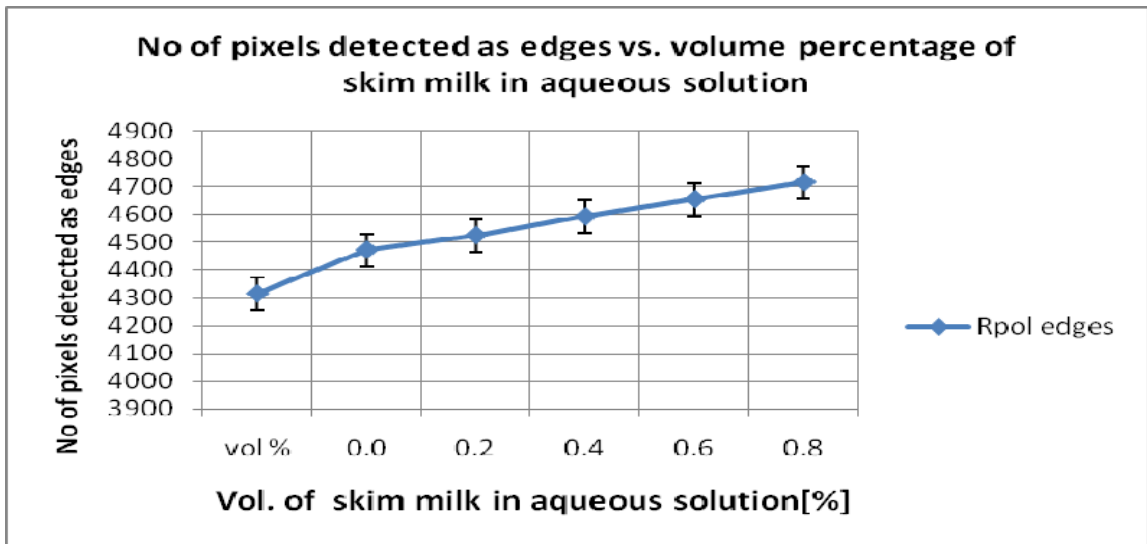


Figure 5.24 Number of pixels detected as edges values for R_{pol} images vs. concentration of volume percentage of skim milk in aqueous solution

In order to highlight the merit of both of techniques, the SBR of Fig.'s 5.13 and 5.23 are plotted together in Fig. 5.25. Similarly, the number of pixels data detected as edges using circular and linear polarized wave interrogation of the phantom (Figs. 5.14 and 5.24), are plotted in Fig. 5.26. The potential of circular wave interrogation of phantoms immersed in scattered media over the linear wave interrogation is highlighted in Fig.'s 5.25 and 5.26, respectively.

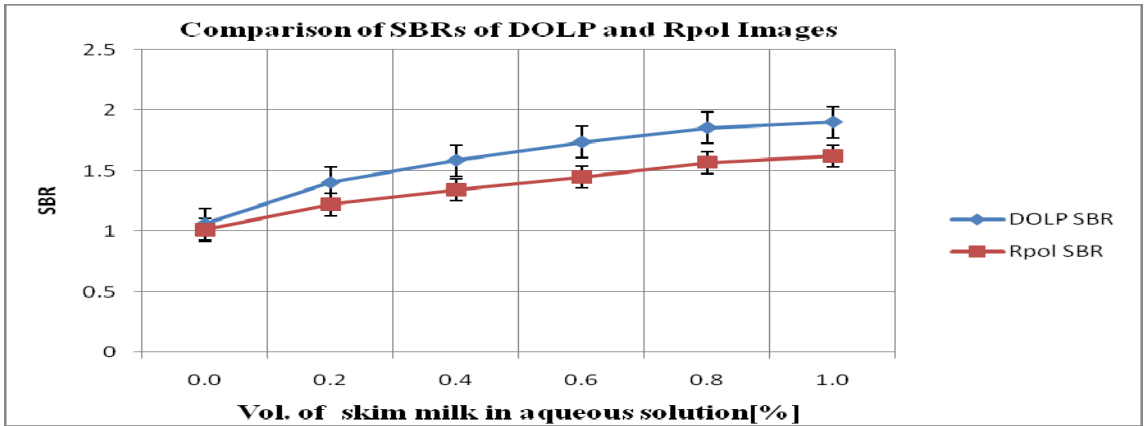


Figure 5.25 Comparison of SBR values of DOLP and R_{pol} images vs. concentration of volume percentage of skim milk in aqueous solution

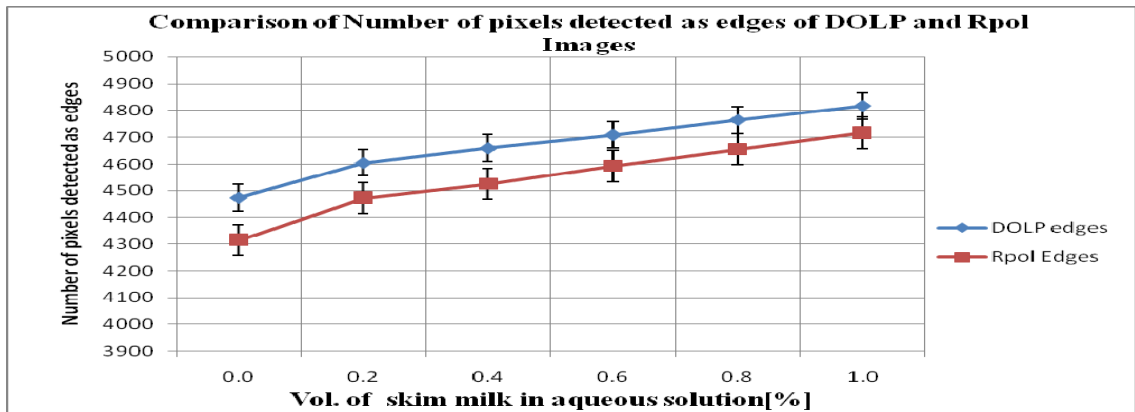


Figure 5.26 Comparison of number of pixels detected as edges of DOLP and R_{pol} images vs. concentration of volume percentage of skim milk in aqueous solution

5.3 Discussion

The null hypotheses discussed in chapter I were tested based on the signal to background ratio values and number of pixels detected as edges in the DOLP, S_0 and R_{pol} images. The experiments were repeated three times to check for repeatability and reproducibility. The null hypotheses was tested by a Model-I Linear Regression Analysis with a type-1 error probability of 0.05 and the Regression Equation was given by

$$\hat{Y} = \alpha + \beta X \quad (5.1)$$

Where \hat{Y} represents the predicted value of dependant variable and X represents the value of independent variable. The regression analysis was done by considering the SBR and number of edges as dependent variable (Y) and concentration of the skim milk solution added as the independent variable (X).

The tables from 5.7 to 5.9 show the source tables for DOLP, S_0 and R_{pol} images obtained when skim milk solution was added in volume percentage increments.

The regression analysis performed on the data by considering number of edges as dependant variable (Y). The tables from 5.10 to 5.13 show the source tables for DOLP, S_0 and R_{pol} images obtained when skim milk solution was added in volume percentage increments.

From the tables 5.7 to 5.9, it can be seen that there exists a significant difference in the signal to background ratios computed for DOLP, S_0 , R_{pol} images with increasing concentrations of skim milk solution.

From the tables 5.10 to 5.13, it can be seen that there exists a significant difference in the number of pixels detected as edges computed for DOLP, S_0 , R_{pol} images with increasing concentrations of skim milk solution.

Table 5.7 Source Table for DOLP SBR values

Source	DF	Sum of Squares	Mean Square	F Value	Pr > F
Regression	1	0.46724	0.46724	49.39029	0.00216
Unexplained	4	0.037841	0.00946		
Total	5	0.505081			
$R^2: 0.92508$					

Table 5.8 Source Table for S_0 SBR values

Source	DF	Sum of Squares	Mean Square	F Value	Pr > F
Regression	1	0.002523	0.002523	115.5029	0.000425
Unexplained	4	8.74E-05	2.18E-05		
Total	5	0.00261			
$R^2: 0.966528$					

Table 5.9 Source Table for R_{pol} SBR values

Source	DF	Sum of Squares	Mean Square	F Value	Pr > F
Regression	1	0.251723	0.251723	117.545	0.000411
Unexplained	4	0.008566	0.002142		
Total	5	0.260289			
$R^2: 0.96709$					

Table 5.10 Source Table for DOLP edges

Source	DF	Sum of Squares	Mean Square	F Value	Pr > F
Regression	1	72043.13	72043.13	99.45606	0.000568
Unexplained	4	2897.486	724.3714		
Total	5	74940.61			
$R^2: 0.9613$					

Table 5.11 Source Table for S₀ edges

Source	DF	Sum of Squares	Mean Square	F Value	Pr > F
Regression	1	23320.46	23320.46	104.1173	0.0005 2
Unexplained	4	895.9302	223.9825		
Total	5	24216.39			
R ² : 0.963003					

Table 5.12 Source Table for R_{pol} edges

Source	DF	Sum of Squares	Mean Square	F Value	Pr > F
Regression	1	98237.6	98237.6	96.14619	0.000606
Unexplained	4	4087.01	1021.752		
Total	5	102324.6			
R ² : 0.960058					

To check for homogeneity of slopes among DOLP, S_0 and R_{pol} regression lines were tested for significance. It can be seen for Table 5.13 that the F-distribution for SBR of DOLP and S_0 , $F(0.05, 1, 8) = 5.32 < F_{observed} = 43.1532419$, implying that there is a significant difference among the regression slopes that were calculated. It can be seen for Table 5.14 that the F-distribution for SBR of DOLP and R_{pol} , $F(0.05, 1, 8) = 5.32 < F_{observed} = 14.1204685$, implying that there is a significant difference among the regression slopes that were calculated. It can be also be seen from Table 5.15 that the F-distribution for number of pixels detected as edges for DOLP and S_0 , $F(0.05, 1, 8) = 5.32 < F_{observed} = 19.0743267$, which implies that there is a significant difference among the regression slopes that were calculated. It can be also be seen from Table 5.16 that the F-distribution for number of pixels detected as edges for DOLP and R_{pol} , $F(0.05, 2, 12) = 5.32 < F_{observed} = 6.022$, which implies that there is a significant difference among the regression slopes that were calculated.

Table 5.13 Source Table Comparing Regression Slopes of DOLP and S_0 images (SBRs)

Source of Variation	df	SS	MS	$F_{observed}$	Significance F
Among b's	1	0.20	0.20	43.1532419	5.32
Average variation within regression	8	0.04	0.04		

Table 5.14 Source Table Comparing Regression Slopes of DOLP and R_{pol} images (SBRs)

Source of Variation	df	SS	MS	$F_{observed}$	Significance F
Variation among regression	1	0.08	0.08	14.1204685	5.32
Average variation within regression	8	0.05	0.05		

Table 5.15 Source Table Comparing Regression Slopes of DOLP and S_0 images (edges)

Source of Variation	df	SS	MS	$F_{observed}$	Significance F
Among b's	1	9044.61	9044.61	19.0743267	5.32
Average variation within regression	8	3793.42	474.177		

Table 5.16 Source Table Comparing Regression Slopes of DOLP and R_{pol} images (Edges)

Source of Variation	df	SS	MS	F _{observed}	Significance F
Variation among regression	1	5258.20	5258.20	6.022707	5.32
Average variation within regression	8	6984.50	873.0619		

A Randomized Complete block (RCB) was used to test for significance between DOLP and R_{pol} images. It was also tested for significance between DOLP and S₀ images. A single factor analysis of variance (ANOVA) blocking on concentration was designed and the statistical model is given by the following equation

$$Y_{ij} = \mu + \alpha_i + \beta_j + \epsilon_{k(ij)} \quad (5.1)$$

Where

- γ_{ijk} : dependent variable
- μ : overall mean response
- α_i : effect due to treatment : Polarization type
- β_j : effect due to treatment (block) : Concentration
- $\epsilon_{k(ij)}$: random error

The analysis showed that there was a significant difference between DOLP and R_{pol} images. The analysis also showed a significant difference between DOLP and S₀

images. The model was tested with a p value of 0.05. The calculations were included in the appendix.

CHAPTER VI

CONCLUSIONS AND FUTURE WORK

This study successfully compared two polarimetric techniques namely the Rotating Retarder Polarimeter method which utilizes circular polarized light and the Linear Polarimeter method which uses linearly polarized light. Both of these experiments were performed using a backscattered polarimetric imaging system. The obtained images from these experiments were computed for Signal to background ratios and Number of pixels detected as edges.

Experimental results from both these techniques showed that the DOLP images obtained by Rotating Retarder Polarimeter method provide better contrast in terms of signal to background ratio (SBR) values and number of pixels detected as edges compared to Degree of Polarization (R_{pol}) images obtained by linear Polarimeter method. Overall, the contributions of this study suggest that the interrogation of targets in turbid media using circularly polarized light exhibits superior imaging characteristics with respect to linearly polarized light interrogation.

The exploration of these methods with different wavelengths, different scattering solutions may yield to further image improvement. The polarimetric techniques can also be explored with biological tissues to assess the capabilities of these methods. Further image processing can also be done to obtain more productive information.

REFERENCES

1. Jeremy C Hebdeny, Simon R Arridgez and David T Delpyy Optical imaging in medicine: I. Experimental techniques University College London, Department of Medical Physics, 11-20 Capper Street, London WC1E 6JA, UK.
2. S. L. Jacques, M. Ostermeyer, L. Wang, and D. Stephens, “Polarized light transmission through skin using video reflectometry: Toward optical tomography of superficial tissue layers,” *Proc. SPIE* 2671.
3. L. T. Perelman, G. I. Zonios, V. Backman, R. Gurjar, I. Itzkan, R. R. Dasari, J. Van Dam, and M. S. Feld, “Quantitative analysis of mucosal tissues in patients using light scattering spectroscopy,” *Proc. SPIE* 3597, 474–479 ~1999.
4. S. G. Demos, H. Savage, A. S. Heerdt, S. Schantz, and R. R. Alfano, “Time resolved degree of polarization for human breast tissue,” *Opt. Commun.* 124, 439–442 ~1996.
5. G. Jarry, O. Schlee, O. Duhamel, J. Virmont, L. Poupinet, B. Clairac, M. Derrien, and D. Yeddou, “Coherent transmission of polarized light through mammalian tissue,” *Proc. SPIE* 2326, 192–201 ~1995.
6. F. C. MacKintosh, J. X. Zhu, D. J. Pine, and D. A. Weitz, “Polarization memory of multiply scattered light,” *Phys. Rev. B* 40~13!, 9342– 9345 ~1989.
7. J. M. Schmitt, A. H. Gandbakhche, and R. F. Bonner, “Use of polarized light to discriminate short-path photons in a multiply scattering medium,” *Appl. Opt.* 31~30!, 6535–6546 ~1992.
8. D. Bicout, C. Brosseau, A. S. Martinez, and J. M. Schmitt, “Depolarization of multiply scattered waves by spherical diffusers: Influence of the size parameter,” *Phys. Rev. E* 49~2!, 1767–1770 ~1994.
9. Ralph E. Nothdurft and Gang Yao,” Effects of turbid media optical properties on object visibility in subsurface polarization imaging”.
10. Steven L.Jacques, Jessica R.Roman, and Ken Lee, “Imaging superficial tissues with polarized light”, *Lasers in Surgery and Medicine*, Vol.26, pp.119-129, 2000.

11. M. J. Raković et al “Measurement and calculation of the two-dimensional backscattering Mueller matrix of a turbid medium”.
12. V. Backman, R. Gurjar, K. Badizadegan, L. Itzkan, R. R. Dasari, L. T. Perelman, and M. S. Feld, “Polarized light scattering spectroscopy for quantitative measurement of epithelial cellular structures in situ,” *IEEE J. Sel. Top. Quantum Electron.* 5, 1019–1026 (1999).
13. N. Yaroslavsky, V. Neel, and R. R. Anderson, “Demarcation of nonmelanoma skin cancer margins in thick excisions using multispectral polarized light imaging,” *J. Investig. Dermatol.* 121, 259–266 (2003).
14. X. H. Ni and R. R. Alfano, “Time-resolved backscattering of circularly and linearly polarized light in a turbid medium,” *Opt. Lett.* 29, 2773–2775 (2004).
15. S. A. Kartazayeva, X. H. Ni, and R. R. Alfano, “Backscattering target detection in a turbid medium by use of circularly and linearly polarized light,” *Opt. Lett.* 30, 1168–1170 (2005).
16. Zharov VP, Ferguson S, Eidt JF, Howard PC, Fink LM, Waner M. Infrared imaging of subcutaneous veins. *Lasers Surg Med* 2004;34:56–61.
17. Anderson RR. Polarized light examination and photography of skin. *Arch Dermatol* 1991;127:1000–1005.
18. Jacques SL, Roman JR, Lee K. Imaging skin pathology with polarized light. *J Biomed Opt* 2002;7(3):329–340.
19. Gnanou F.Sudha, Theerta G.Palanivelu, “Polarimetric imaging of subsurface tissue-numerical results”, *Journal of Biomedical Optics*, Vol.10, No.5, pp.054014-1 to 054014-8, September/October 2005.
20. H. Hielscher, A. A. Eick, J. R. Mourant, D. Shen, J. P. Freyer, and I. J. Bigio, “Diffuse backscattering Mueller matrices of highly scattering media,” *Opt. Express* 1, 441–453.
21. J.S. Baba, J.R. Chung, A.H. DeLaughter, B.D. Cameron and G.L. Cote’, “Development and calibration of an automated Mueller matrix polarization imaging system”, *Journal of Biomedical Optics*, Vol. 7, No. 3, pp.341-349, July 2002.
22. Ajaina Nezhuvungal, Yanfang Li, Harini Anumula, and Brent D. Cameron Biomedical Optics Laboratory, University of Toledo, “Mueller Matrix Optical Imaging with Application to Tissue Diagnostics”.
23. Francois Goudail, Patrick Terrier, Yoshitate Takakura, Laurent Bigue, Frederic Galland, and Vincent Devlaminck, “Target detection with a liquid-crystal-based

- passive Stokes polarimeter”, *Applied Optics*, Vol.43, No.2, pp.274-282, January 10, 2004.
24. G.C.Giakos, “Active Backscattered Optical Polarimetric Imaging of Scattered Targets”, *Proceedings of the IEEE Instrumentation and Measurement Technology Conference*, Vol.1, pp.430-432, May 18-20, 2004.
 25. G.C.Giakos, “Novel Multifusion Optical Imaging Sensing Principles”, *Proceedings of the IEEE Instrumentation and Measurement Technology Conference*, Vol.1, pp.756-759, May 18-20, 2004.
 26. G.C.Giakos, “Laser Imaging through Scattering Media”, *Proceedings of the IEEE Instrumentation and Measurement Technology Conference*, Vol.1, pp.433-437, May 18-20, 2004.
 27. G.C.Giakos, “Multifusion Multispectral Light-wave Polarimetric Detection Principles and Systems”, *IEEE Transactions on Instrumentation and Measurement*, Vol.55, No.6, pp.1904-1912, December 2006.
 28. G.C.Giakos, “New Pathways towards the Enhancement of the Image Quality”, *Proceedings of the IEEE Instrumentation and Measurement Technology Conference*, pp.1-5, May 1-3, 2005.
 29. G.C.Giakos et al, “Enhanced Detection and Imaging based on Novel Molecular Nanophotonics Principles”, *IEEE International Workshop on Imaging Systems and Techniques*, Krakow, Poland, May 4-5, 2007.
 30. R.M.A.Azzam, “Photopolarimetric measurement of the Mueller matrix by Fourier analysis of a single detected signal”, *Optics Letters*, Vol.2, No.6, pp.148-150, June 1978.
 31. Dennis H.Goldstein, “Mueller matrix dual rotating retarder polarimeter”, *Applied Optics*, Vol.31, No.31, pp.6676-6683, November 1, 1992.
 32. Matthew H.Smith, “Optimization of a dual-rotating-retarder Mueller matrix polarimeter”, *Applied Optics*, Vol.41, No.13, pp.2488-2493, May 1, 2002.
 33. D.B.Chenault and J.L.Pezzaniti, “Polarization imaging through scattering media”, *Proceedings of the SPIE*, Vol.4133, 2000.
 34. Polarization-degree imaging contrast in turbid media: a quantitative study Hanrong Shao, Yonghong He, Wei Li, and Hui Ma.
 35. Cameron, B.D., et al., "Measurement and calculation of the two-dimensional backscattering Mueller matrix of a turbid medium; errata", *Optics Letters*, 23, (1630), 1998.

36. Jerry E.Solomon, "Polarization Imaging", *Applied Optics*, Vol.20, no.9, pp.1537-1544, May 1, 1981.
37. P.C.Y.Chang, J.G.Walker, K.I.Hopcraft, B.Ablitt, E.Jakeman, "Polarization discrimination for active imaging in scattering media", *Optics Communications*, Vol.159, pp.1-6, January 1, 1999.
38. J.M.Schmitt, A.H.Gandjbakche, and R.F.Bonner, "Use of polarized light to discriminate short-path photons in a multiply scattering medium", *Applied Optics*, Vol.31, No.30, pp.6535-6545, October 20, 1992.
39. J.S.Tyo, M.P.Rowe, E.N.Pugh, Jr., and N.Engheta, "Target detection in optically scattering media by polarization-difference imaging", *Applied Optics*, Vol.35, No.11, pp.1855-1870, April 10, 1996.
40. Gang Yao and Lihong V.Wang, "Propagation of polarized light in turbid media: simulated animation sequences", *Optics Express*, Vol.7, No.5, pp.198-203, August 28, 2000.
41. Manuela Lualdi, Ambrogio Colombo, Bruno Farina, Stefano Tomatis and Renato Marchesini, "A phantom with tissue-like optical properties in the visible and near infrared for use in photomedicine", *Lasers in Surgery and Medicine*, Vol.28, pp.237-243, 2001.
42. Piero Brusaglioni, Giovanni Zaccanti, and Qingnong Wei, "Transmission of a pulsed polarized light beam through thick turbid media: numerical results", *Applied Optics*, Vol.32, No.30, pp.6142-6150, October 20, 1993.
43. G.C. Holdren, "Biological Aspects of Turbidity and Other Optical Properties of Water", *Turbidity and other sediment surrogates workshop*, Reno, NV, April 30th May 2nd 2002.
44. V. Sankaran, J. T. Walsh, Jr., and D. J. Maitland, "Comparative study of polarized light propagation in biological tissues," *J. Biomed. Opt.* 7, 300 – 306 (2002).
45. Keerthi Valluru, "Study of Biomolecular Optical Signatures For Early Disease Detection and Cell Physiology Monitoring".
46. Sobel, I., Feldman,G., "A 3x3 Isotropic Gradient Operator for Image Processing", presented at a talk at the Stanford Artificial Project in 1968, unpublished but often cited, orig. in *Pattern Classification and Scene Analysis*, Duda,R. and Hart,P., John Wiley and Sons,'73, pp271-2
47. Rod Nave."Hyper-physics".<http://hyperphysics.phastr.gsu.edu/hbase/phyopt/polclas> Georgia State University.

APPENDIX

Comparison of Slopes for DOLP and S_0 images for signal to background ratios (SBR s)

Skim Milk	DOLP	So
Σni	6	6
a(no. of groups)	6	6
Σx^2	0.70	0.7
Σxy	0.57	0.042022
Σy^2	0.51	0.00261
$\Sigma d^2y.x$	0.04	8.74E-05
SSamong	0.47	0.002523
SSwithin	0.04	8.74E-05
by.x	0.82	0.060031
Ybar	1.59	0.53716
Xbar	0.50	0.5
a(Y intercept)	1.18	0.507144
(b-b bar)	0.32	-0.4322
(b-b bar) ²	0.11	0.186799
$\Sigma x^2 (b-b \text{ bar})^2$	0.07	0.130759

Test of equality among K regression coefficients

K	2
$\Sigma\Sigma xy$	0.61
$\Sigma\Sigma x^2$	1.40
Bbar	0.438515
SSamong b's	0.20
MSamong b's	0.20459
$\Sigma\Sigma d^2y.x$	0.04
($\Sigma a - 2k$)	8
$s^2y.x$	0.004741

Comparison of Slopes for DOLP and S_0 images for pixels detected as edges

Skim Milk	DOLP	So
Σn_i	6	6
a(no. of groups)	6	6
Σx^2	0.70	0.7
Σxy	224.57	127.7667
Σy^2	74940.61	24216.39
$\Sigma d^2_{y.x}$	2897.49	895.9302
SSamong	72043.13	23320.46
SSwithin	2897.49	895.9302
$b_{y.x}$	320.81	182.5238
Ybar	4672.17	3788.5
Xbar	0.50	0.5
a(Y intercept)	4511.76	3697.238
(b-b bar)	69.14	-69.1429
(b-b bar) ²	4780.73	4780.735
$\Sigma x^2 (b-b \text{ bar})^2$	555.04	8489.567

Test of equality among K regression coefficients

K	2
$\Sigma \Sigma xy$	352.33
$\Sigma \Sigma x^2$	1.40
Bbar	251.6667
SSamong b's	9044.61
MSamong b's	9044.607
$\Sigma \Sigma d^2_{y.x}$	3793.42
($\Sigma a - 2k$)	8
$s^2_{y.x}$	474.177

Comparison of Slopes for DOLP and R_{pol} images for signal to background ratios (SBR s)

a(no. of groups)	6	6
Σx^2	0.70	0.7
Σxy	0.57	0.419769
Σy^2	0.51	0.260289
$\Sigma d^2y.x$	0.04	0.008566
SSamong	0.47	0.251723
SSwithin	0.04	0.008566
$b_{y.x}$	0.82	0.59967
Ybar	1.59	1.368526
Xbar	0.50	0.5
a(Y intercept)	1.18	1.068691
(b-b bar)	0.32	0.107437
(b-b bar) ²	0.11	0.011543
$\Sigma x^2 (b-b bar)^2$	0.07	0.00808

Test of equality among K regression coefficients

K	2
$\Sigma \Sigma xy$	0.99
$\Sigma \Sigma x^2$	1.40
Bbar	0.708334
SSamong b's	0.08
MSamong b's	0.081911
$\Sigma \Sigma d^2y.x$	0.05
($\Sigma a - 2k$)	8
$S^2_{y.x}$	0.005801

Comparison of Slopes for DOLP and R_{pol} images for pixels detected as edges

Skim Milk	DOLP	R _{pol}
Σn_i	6	6
a(no. of groups)	6	6
Σx^2	0.70	0.7
Σxy	224.57	262.2333
Σy^2	74940.61	102324.6
$\Sigma d^2_{y.x}$	2897.49	4087.01
SS _{among}	72043.13	98237.6
SS _{within}	2897.49	4087.01
$b_{y.x}$	320.81	374.619
Y _{bar}	4672.17	4546.5
X _{bar}	0.50	0.5
a(Y intercept)	4511.76	4359.19
(b-b _{bar})	-26.90	26.90476
(b-b _{bar}) ²	723.87	723.8662
$\Sigma x^2 (b-b_{bar})^2$	555.04	4703.156

Test of equality among K regression coefficients

K	2
$\Sigma \Sigma xy$	486.80
$\Sigma \Sigma x^2$	1.40
B _{bar}	347.7143
SS _{among b's}	5258.20
MS _{among b's}	5258.196
$\Sigma \Sigma d^2_{y.x}$	6984.50
($\Sigma a - 2k$)	8
$S^2_{y.x}$	873.0619

Calculations for DOLP image signal to background ratios (SBRs)

skim milk	X	Y	x = X - Xbar	y = Y - Ybar	x ²	xy	y ²
	0.0	1.061326	-0.5	-0.52984	0.25	0.26492	0.280731
	0.2	1.402588	-0.3	-0.18858	0.09	0.056574	0.035562
	0.4	1.586522	-0.1	-0.00464	0.01	0.000464	2.16E-05
DOLP	0.6	1.737644	0.1	0.146477	0.01	0.014648	0.021456
SBR	0.8	1.856169	0.3	0.265002	0.09	0.079501	0.070226
	1.0	1.902751	0.5	0.311584	0.25	0.155792	0.097085
SUM	3.0	9.547	0.0	0.0	0.7	0.571899	0.505081
MEAN	0.5	1.591167					
sum/n-1					0.14	0.11438	0.101016
sum/n-2							

Yhat = a + bx	Dy*x	d ² (y*x)	yhat = Yhat - Ybar	yhat ²	x ² (b-b bar) ²
1.18266756	-0.1213415	0.0147238	-0.408499164	0.166872	0.026368078
1.34606723	0.05652076	0.0031946	-0.245099499	0.060074	0.009492508
1.50946689	0.07705551	0.0059376	-0.081699833	0.006675	0.001054723
1.67286656	0.06477759	0.0041961	0.081699833	0.006675	0.001054723
1.83626623	0.01990261	0.0003961	0.245099499	0.060074	0.009492508
1.99966589	-0.096915	0.0093925	0.408499164	0.166872	0.026368078
9.54700037	2.2204E-16	0.0378407	-4.44089E-16	0.46724	0.073830617
1.59116673					
		0.0094602			

Calculations for S_0 image signal to background ratios (SBRs)

skim milk	X	Y	x = X - Xbar	y = Y - Ybar	x ²	xy	y ²
	0.0	0.501193	-0.5	-0.03597	0.25	0.017983	0.001294
	0.2	0.522309	-0.3	-0.01485	0.09	0.004455	0.000221
	0.4	0.534419	-0.1	-0.00274	0.01	0.000274	7.51E-06
s0	0.6	0.547277	0.1	0.010117	0.01	0.001012	0.000102
SBR	0.8	0.554274	0.3	0.017114	0.09	0.005134	0.000293
	1.0	0.563486	0.5	0.026327	0.25	0.013163	0.000693
SUM	3.0	3.222958	0.0	0.0	0.7	0.042022	0.00261
MEAN	0.5	0.53716					
sum/n-1					0.14	0.008404	0.000522
sum/n-2							

Yhat = a + Bx	dy*x	d ² (y*x)	yhat= Yhat - Ybar	yhat ²	x2 (b-b bar) ²
0.50714402	-0.005951	3.541E-05	-0.030015614	0.000901	0.0467
0.51915027	0.003159	9.977E-06	-0.018009369	0.000324	0.016812
0.53115652	0.003262	1.064E-05	-0.006003123	3.6E-05	0.001868
0.54316276	0.004114	1.692E-05	0.006003123	3.6E-05	0.001868
0.55516901	-0.000895	8.01E-07	0.018009369	0.000324	0.016812
0.56717525	-0.003689	1.361E-05	0.030015614	0.000901	0.0467
3.22295784	0.000000	8.736E-05	-2.22045E-16	0.002523	0.130759
0.53715964					

Calculations for R_{pol} image signal to background ratios (SBRs)

skim milk	X	Y	$x = X - Xbar$	$y = Y - Ybar$	x^2	xy	y^2
	0.0	1.010312	-0.5	-0.35821	0.25	0.179107	0.128317
	0.2	1.222074	-0.3	-0.14645	0.09	0.043936	0.021448
	0.4	1.342443	-0.1	-0.02608	0.01	0.002608	0.00068
Rpol	0.6	1.447211	0.1	0.078685	0.01	0.007869	0.006191
SBR	0.8	1.567437	0.3	0.198911	0.09	0.059673	0.039565
	1.0	1.62168	0.5	0.253153	0.25	0.126577	0.064087
SUM	3.0	8.211158	0.0	0.0	0.7	0.419769	0.260289
MEAN	0.5	1.368526					
Sum/n-1					0.14	0.083954	0.052058
Sum/n-2							

$\hat{Y} = a + bx$	$dy * x$	$d^2(y * x)$	$\hat{y} = \hat{Y} - Ybar$	\hat{y}^2	$x^2 (b - bbar)^2$
1.06869107	-0.058379	0.0034081	-0.299835202	0.089901	0.002886
1.18862515	0.033449	0.0011189	-0.179901121	0.032364	0.001039
1.30855923	0.033884	0.0011481	-0.05996704	0.003596	0.000115
1.42849332	0.018718	0.0003504	0.05996704	0.003596	0.000115
1.5484274	0.019010	0.0003614	0.179901121	0.032364	0.001039
1.66836148	-0.046682	0.0021792	0.299835202	0.089901	0.002886
8.21115765	0.000000	0.008566	0	0.251723	0.00808
1.36852627					
		0.0021415			

Calculations for DOLP image Number of pixels detected as edges

skim milk	X	Y	x = X- Xbar	y =Y- Ybar	x^2	xy	y^2
	0.0	4474.667	-0.5	-197.5	0.25	98.75	39006.25
	0.2	4605.667	-0.3	-66.5	0.09	19.95	4422.25
	0.4	4660	-0.1	-12.1667	0.01	1.216667	148.0278
DOLPedge	0.6	4709.333	0.1	37.16667	0.01	3.716667	1381.361
	0.8	4765	0.3	92.83333	0.09	27.85	8618.028
	1.0	4818.333	0.5	146.1667	0.25	73.08333	21364.69
SUM	3.0	28033	0.0	0.0	0.7	224.5667	74940.61
MEAN	0.5	4672.167					
sum/n-1					0.14	44.91333	14988.12
sum/n-2							

Yhat = a +bx	dy*x	d^2(y*x)	yhat= Yhat- Ybar	yhat^2	x2 (b-b bar)2
4511.7619	-37.095238	1376.0567	-160.4047619	25729.69	198.2285
4575.92381	29.7428571	884.63755	-96.24285714	9262.688	71.36227
4640.08571	19.9142857	396.57878	-32.08095238	1029.188	7.929141
4704.24762	5.08571429	25.86449	32.08095238	1029.188	7.929141
4768.40952	-3.4095238	11.624853	96.24285714	9262.688	71.36227
4832.57143	-14.238095	202.72336	160.4047619	25729.69	198.2285
28033	-1.819E-12	2897.4857	0	72043.13	555.0399
4672.16667					
		724.37143			

Calculations for S_0 number of pixels detected as edges

skim milk	X	Y	$x = X - \bar{X}$	$y = Y - \bar{Y}$	x^2	xy	y^2
	0.0	3676.667	-0.5	-111.833	0.25	55.91667	12506.69
	0.2	3749.667	-0.3	-38.8333	0.09	11.65	1508.028
	0.4	3780.333	-0.1	-8.16667	0.01	0.816667	66.69444
S0edge	0.6	3813	0.1	24.5	0.01	2.45	600.25
	0.8	3839.667	0.3	51.16667	0.09	15.35	2618.028
	1.0	3871.667	0.5	83.16667	0.25	41.58333	6916.694
SUM	3.0	22731	0.0	0.0	0.7	127.7667	24216.39
MEAN	0.5	3788.5					
sum/n-1					0.14	25.55333	4843.278
sum/n-2							

$\hat{Y} = a + bx$	$dy * x$	$d^2(y * x)$	$\hat{y} = \hat{Y} - \bar{Y}$	\hat{y}^2	$x^2 (b - \bar{b})^2$
3697.2381	-20.571429	423.18367	-91.26190476	8328.735	3031.988
3733.74286	15.9238095	253.56771	-54.75714286	2998.345	1091.516
3770.24762	10.0857143	101.72163	-18.25238095	333.1494	121.2795
3806.75238	6.24761905	39.032744	18.25238095	333.1494	121.2795
3843.25714	-3.5904762	12.891519	54.75714286	2998.345	1091.516
3879.7619	-8.0952381	65.53288	91.26190476	8328.735	3031.988
22731	-1.364E-12	895.93016	9.09495E-13	23320.46	8489.567
3788.5					
		223.98254			

Calculations for R_{pol} number of pixels detected as edges

skim milk	X	Y	$x = X - \bar{X}$	$y = Y - \bar{Y}$	x^2	xy	y^2
	0.0	4315.333	-0.5	-231.167	0.25	115.5833333	53438.03
	0.2	4473	-0.3	-73.5	0.09	22.05	5402.25
	0.4	4525.333	-0.1	-21.1667	0.01	2.116666667	448.0278
Rpoledge	0.6	4593	0.1	46.5	0.01	4.65	2162.25
	0.8	4655.667	0.3	109.1667	0.09	32.75	11917.36
	1.0	4716.667	0.5	170.1667	0.25	85.08333333	28956.69
SUM	3.0	27279	0.0	0.0	0.7	262.2333333	102324.6
MEAN	0.5	4546.5					
Sum/n-1					0.14	52.44666667	20464.92
Sum/n-2							

$\hat{Y} = a + bx$	$dy * x$	$d^2(y * x)$	$\hat{y} = \hat{Y} - \bar{Y}$	\hat{y}^2	$x^2 (b - \bar{b})^2$
4359.190476	-43.857143	1923.449	-187.3095238	35084.86	1679.699
4434.114286	38.8857143	1512.0988	-112.3857143	12630.55	604.6915
4509.038095	16.2952381	265.53478	-37.46190476	1403.394	67.18795
4583.961905	9.03809524	81.687166	37.46190476	1403.394	67.18795
4658.885714	-3.2190476	10.362268	112.3857143	12630.55	604.6915
4733.809524	-17.142857	293.87755	187.3095238	35084.86	1679.699
27279	-2.728E-12	4087.0095	22732.5	98237.6	4703.156
4546.5					
		1021.7524			

Program to test for significance between The Rotating Retarder Polarimeter method and The Linear Polarimeter method (SBR)

```
data;  
input polarization $ conc $ @;  
do i = 1 to 3;  
input SBR @@;  
output;  
end;  
cards;  
DOLP 0.0 1.07186 1.06409 1.04801  
DOLP 0.2 1.36658 1.39914 1.44203  
DOLP 0.4 1.56118 1.59637 1.60200  
DOLP 0.6 1.73788 1.73300 1.73764  
DOLP 0.8 1.84708 1.84951 1.87190  
DOLP 1.0 1.90187 1.89225 1.91412  
RPOL 0.0 0.98375 1.01509 1.03209  
RPOL 0.2 1.22458 1.22093 1.22207  
RPOL 0.4 1.34354 1.34168 1.34209  
RPOL 0.6 1.44411 1.45040 1.44712  
RPOL 0.8 1.57196 1.55165 1.57869  
RPOL 0.0 1.61676 1.62442 1.62384  
;  
proc glm;  
class polarization conc;  
model SBR=polarization conc;
```

Output statistics

The GLM Procedure

Dependent Variable: SBR

Source	DF	Sum of Squares	Mean Square	F Value	Pr > F
Model	6	2.67339166	0.44556528	178.72	<.0001
Error	29	0.07229827	0.00249304		
Corrected Total	35	2.74568993			

R-Square	Coeff Var	Root MSE	SBR Mean
0.973668	3.374227	0.049930	1.479758

Source	DF	Type I SS	Mean Square	F Value	Pr > F
polarization	1	0.44483120	0.44483120	178.43	<.0001
conc	5	2.22856046	0.44571209	178.78	<.0001

Source	DF	Type III SS	Mean Square	F Value	Pr > F
polarization	1	0.44483120	0.44483120	178.43	<.0001
conc	5	2.22856046	0.44571209	178.78	<.0001

Program to test for significance between The Rotating Retarder Polarimeter method and The Linear Polarimeter method (Number of pixels detected as edges)

```
data;  
input polarization $ conc $ @;  
do i = 1 to 3;  
input SBR @@;  
output;  
end;  
cards;  
DOLP 0.0 4305 4340 4326  
DOLP 0.2 4581 4598 4638  
DOLP 0.4 4640 4665 4675  
DOLP 0.6 4660 4684 4784  
DOLP 0.8 4700 4742 4853  
DOLP 1.0 4744 4825 4866  
Rpol 0.0 4275 4382 4289  
Rpol 0.2 4605 4411 4403  
Rpol 0.4 4637 4486 4453  
Rpol 0.6 4663 4523 4593  
Rpol 0.8 4724 4573 4670  
Rpol 1.0 4752 4713 4685  
;  
proc glm;  
class polarization conc;  
model SBR=polarization conc;
```

Output statistics

The GLM Procedure

Dependent Variable: SBR

Source	DF	Sum of Squares	Mean Square	F Value	Pr > F
Model	6	833321.8333	138886.9722	32.39	<.0001
Error	29	124367.8056	4288.5450		
Corrected Total	35	957689.6389			

R-Square	Coeff Var	Root MSE	SBR Mean
0.870138	1.424809	65.48698	4596.194

Source	DF	Type I SS	Mean Square	F Value	Pr > F
polarization	1	88903.3611	88903.3611	20.73	<.0001
conc	5	744418.4722	148883.6944	34.72	<.0001

Source	DF	Type III SS	Mean Square	F Value	Pr > F
polarization	1	88903.3611	88903.3611	20.73	<.0001
conc	5	744418.4722	148883.6944	34.72	<.0001

Program to test for significance between DOLP and S₀ images (SBR)

```
data;
input polarization $ conc $ @;
do i = 1 to 3;
input SBR @@;
output;
end;
cards;
DOLP 0.0 1.07186 1.06409 1.04801
DOLP 0.2 1.36658 1.39914 1.44203
DOLP 0.4 1.56118 1.59637 1.60200
DOLP 0.6 1.73788 1.73300 1.73764
DOLP 0.8 1.84708 1.84951 1.87190
DOLP 1.0 1.90187 1.89225 1.91412
S0 0.0 0.51746 0.49300 0.49311
S0 0.2 0.53688 0.51346 0.51657
S0 0.4 0.54839 0.54264 0.51222
S0 0.6 0.56513 0.55605 0.52063
S0 0.8 0.57394 0.56246 0.52640
S0 1.0 0.58137 0.56964 0.56348
;
proc glm;
class polarization conc;
model SBR=polarization conc;
```

Output statistics

The GLM Procedure

Dependent Variable: SBR

Source	DF	Sum of Squares	Mean Square	F Value	Pr > F
Model	6	10.84574569	1.80762428	80.08	<.0001
Error	29	0.65463786	0.02257372		
Corrected Total	35	11.50038354			

R-Square	Coeff Var	Root MSE	SBR Mean
0.943077	14.11149	0.150246	1.064704

Source	DF	Type I SS	Mean Square	F Value	Pr > F
polarization	1	9.96841700	9.96841700	441.59	<.0001
conc	5	0.87732869	0.17546574	7.77	<.0001

Source	DF	Type III SS	Mean Square	F Value	Pr > F
polarization	1	9.96841700	9.96841700	441.59	<.0001
conc	5	0.87732869	0.17546574	7.77	<.0001

Program to test for significance between DOLP and S_0 images (Number of pixels detected as edges)

```
data;  
input polarization $ conc $ @;  
do i = 1 to 3;  
input SBR @@;  
output;  
end;  
cards;  
DOLP 0.0 4305 4340 4326  
DOLP 0.2 4581 4598 4638  
DOLP 0.4 4640 4665 4675  
DOLP 0.6 4660 4684 4784  
DOLP 0.8 4700 4742 4853  
DOLP 1.0 4744 4825 4866  
S0 0.0 3609 3689 3732  
S0 0.2 3752 3763 3734  
S0 0.4 3767 3775 3799  
S0 0.6 3784 3801 3854  
S0 0.8 3800 3864 3855  
S0 1.0 3836 3896 3883  
;  
proc glm;  
class polarization conc;  
model SBR=polarization conc;
```

Output Statistics

The GLM Procedure

Dependent Variable: SBR

Source	DF	Sum of Squares	Mean Square	F Value	Pr > F
Model	6	7056128.500	1176021.417	254.03	<.0001
Error	29	134255.139	4629.488		
Corrected Total	35	7190383.639			

R-Square	Coeff Var	Root MSE	SBR Mean
0.981329	1.613403	68.04034	4217.194

Source	DF	Type I SS	Mean Square	F Value	Pr > F
polarization	1	6616041.361	6616041.361	1429.11	<.0001
conc	5	440087.139	88017.428	19.01	<.0001

Source	DF	Type III SS	Mean Square	F Value	Pr > F
polarization	1	6616041.361	6616041.361	1429.11	<.0001
conc	5	440087.139	88017.428	19.01	<.0001